AN ABSTRACT OF THE THESIS OF

Jeffrey A. Norris for the degree of Master of Science in Mechanical Engineering presented on February 23, 1996. Title: Properties of a Niobium-Titanium Multilayer Thin Film.

Redacted for privacy

Abstract approved: _____

William H. Warnes

A multilayer thin film of niobium (Nb) and titanium (Ti) with bilayer period of 135.8Å and Nb:Ti thickness ratio of 0.57 was made by DC magnetron sputtering onto Silicon substrates in the first stage of modeling the two-phase flux pinning microstructure of conventional NbTi alloys. The critical temperature (T_c) was depressed below 4.2 K due to proximity effect coupling and crystal disorder.

An explicit finite difference based computer diffusion program was written to model the interdiffusion of the multilayer as a function of time and temperature. Based on the results of the diffusion model, heat treatments at 300°C, 400°C, and 450°C for 1, 3, & 10 hours, and 600°C for 1 hour were conducted to first recrystallize the multilayer, and then cause progressive interdiffusion. The predicted thickness of the alloy interlayer created by interdiffusion was used to predict T_c based on a proximity effect coupling theory.

Low and high angle X-ray diffraction was conducted to measure the multilayer structure, lattice parameter, and phase coherence for all samples. The multilayer structure was stable up to 10 hours at 450°C. The 600°C heat treatment completely interdiffused the multilayer. Transmission electron microscopy was conducted to confirm the multilayer structure and the bilayer period. Selected Area Diffraction also showed increased order with heat treatment.

The resistivity of all samples was measured at 298 K, 77.2 K, and 4.2 K. The $\frac{\partial \rho}{\partial T}$ of all samples was negative between 298 K and 77 K, and positive between 77 K and 4.2 K. The T_c, H_{c2}, and J_c were measured for samples with T_c above 4.2 K. Samples at 3 and 10 hours at 400°C and samples at 1 and 3 hours at 400°C showed T_c's at or near 4.2 K. The sample at 10 hours at 450°C had a T_c of 5.5K. The fully interdiffused 1 hour at 600°C sample had a T_c of 7.6 K. The H_{c2} of the superconducting samples increased with increasing heat treatment. The T_c's predicted from the diffusion model follow the general trend of the empirical results.

Properties of a Niobium-Titanium Multilayer Thin Film

by

Jeffrey A. Norris

A THESIS

submitted to

Oregon State University

in partial fulfillment of

the requirements for the

degree of

Master of Science

Completed February 23, 1996

Commencement June 1996

Master of Science thesis of Jeffrey A. Norris presented on February 23, 1996

APPROVED:

Redacted for privacy

Major Professor, representing Mechanical Engineering

Redacted for privacy

Chair of Department of Mechanical Engineering

Redacted for privacy

Dean of Graduate School

I understand that my thesis will become part of the permanent collection of Oregon State University libraries. My signature below authorizes release of my thesis to any reader upon request.

Redacted for privacy

Jeffrey A. Norris, Author

ACKNOWLEDGMENT

I would like to express my thanks to my advisor and friend, Dr. Bill Warnes, for all his support. Though he was on sabbatical in Boston for a year, he maintained open lines of communication. His encouragement and insight helped me through many of the long hours of trying to figure out what in the world was going on with this project.

My thanks go to Kenny Faase for his work on the TEM and Proximity coupling theories. He blazed a path though the hairy equations, where I was too chicken to go. Good job Kenny. Without his trail to follow, they would have made no sense to me. I also appreciate the advice he gave that helped me get this thesis written. Special thanks also go to Dr. Vidya Kaushik of Motorola for providing TEM images.

I would like to thank Dr. Pattee for her help on diffusion. She made sure I maintained conservation of mass, which in turn conserved my sanity. Thanks also go to Dr. Paasch for his help when I re-wrote the diffusion computer code from QuickBasic to C on the UNIX Workstation.

I would like to give special thanks to Pat Woodward in the Chemistry Department at Oregon State University for all of his help and time in explaining X-ray diffraction, as well as helping me take measurements. Though his time was limited, he graciously gave everything I needed. Thanks Pat. Good luck in your work!

I would like to thank Goran Karapetrov in the Physics department at Oregon State University for his help and friendship. Thank you for working with me through several long nights to get T_c measurements. I will not forget you, my friend.

Special thanks go to Dr. Joe Glaser and Ralph Pombo at Lawrance Livermore National Laboratory, for making our films, and for putting up with our slow progress. Thanks also go to the Department of Energy for funding this project under grant number DE-FG06-93ER40804.

I want to thank my wife Reneé for her patience, understanding, and support through the long days and nights. We made it! Last, but not least, I give the glory, honor and thanks to Jesus Christ, my Lord and Savior.

TABLE OF CONTENTS

TABLE OF CONTENTS (Continued)

LIST OF FIGURES

LIST OF FIGURES (Continued)

LIST OF TABLES

Properties of a Niobium-Titanium Multilayer Thin Film

1. INTRODUCTION

Multilayered thin film materials have been studied for their unique properties and uses in X-ray mirrors, quantum well semiconductors, and superconductivity. In this thesis, my goal is to characterize a multilayer thin film of Niobium and Titanium designed for superconductivity research.

This multilayer was made with the hopes that it would exhibit measurable superconducting properties. To our surprise, it did not. The fact that it took us several months to convince ourselves that we were using the right techniques only added to the problem. This thesis chronicles the characterization of the multilayer and the experiments carried out to improve its properties in the hopes that everything learned here will allow better samples to be made in the coming years.

1.1 Magnetic Flux Penetration of Type II Superconductors

The Ginzburg-Landau (1950) theory of superconductivity is based on a macroscopic quantum mechanical wave function (commonly called the order parameter),

$$|\Psi(\sigma)|^2 = n_s, \qquad [1.1]$$

where n_s is the density of superconducting electrons, and σ is the spatial coordinate system. The temperature dependent distance over which the order parameter changes is

called the coherence length, $\xi(T)$. This material dependent distance defines how the order parameter changes from zero (the normal or non-superconducting state) to 1, its maximum value in the superconductor. The Bardeen, Cooper, and Schrieffer (BCS) theory (1957) and work by Frohlich (1950) successfully described superconductivity as a coupling of electrons through a weak attraction due to an electron-phonon interaction.

Superconductivity and its properties of zero resistance and perfect diamagnetism are limited by the three parameters of temperature, current density, and magnetic field. Diamagnetic behavior results from currents that flow in a thin layer at the boundary of the superconductor, preventing the externally applied magnetic field from penetrating into the bulk of the superconductor. The current density in this layer is not infinite, so the magnetic field penetrates a characteristic distance, λ, the penetration depth.

In a Type II superconductor, the perfect diamagnetic behavior exists up to a low critical field (H_{c1}). At field strengths above H_{c1}, the thermodynamically stable state allows penetration of magnetic flux into the bulk of the superconductor in the form of discrete, cylindrical flux quanta (fluxons) arranged in a two-dimensional, triangular lattice (Flux Line Lattice or FFL). (Abrikosov, 1957, Essman and Trauble, 1967) The spacing between fluxons is given by

$$d = \sqrt{\frac{h}{\sqrt{3}eB}} \qquad [1.2]$$

where h is Plank's Constant in *Joule seconds*, e is the charge of an electron in *Coulombs*, and B is the magnetic flux density, in *Tesla*.

Superconducting properties can be destroyed by high magnetic fields, high temperature, and high current densities. The critical temperature (T_c) and the critical magnetic fields (H_c, H_{c1}, and H_{c2}) are material properties that change little due to processing or microstructure for a particular composition. However, superconducting materials have shown critical current densities (J_c) that vary over several orders of magnitude due to changes in microstructure and defect density.

When a current is passed through the superconductor, the fluxons will experience a Lorentz force, given by,

$$\vec{F}_L = \vec{J} \times \vec{B} \qquad [1.2]$$

The Lorentz force will move fluxons unless they are located at sites in which they may resist the force. (Ullmaier, 1975) The motion of fluxons through the superconductor induces an electric field, which results in a resistive power loss. Heating turns the superconductor into a normal metal and therefore destroys the superconductivity of the material. Regions of compositional non-uniformity or second phase precipitates reduce the volume free energy of the fluxon in the superconducting material as a function of fluxon position. These are sites which fluxons preferentially occupy.(Campbell and Evetts, 1972, Dew-Hughes, 1974, Zerweck, 1981) A fluxon located at such a site will be able to resist a Lorentz force with a pinning force, much like an atomic dislocation impeded by a precipitate. The fluxon will not move until the critical current density (J_c) produces a Lorentz force large enough to induce flux flow. Flux pinning increases the maximum current density that can be passed through a superconductor.(Larbalestier, 1981)

1.2 Motivation

The α-titanium precipitates in conventionally processed niobium-titanium (NbTi) wires are the source of the large pinning strengths in these materials.(Larbalestier, 1981, Meingast *et al*, 1989) The arrangement of these precipitates, however, is random, unlike the Flux Line Lattice. Artificial pinning centers have recently been studied in an attempt to understand flux pinning by spacing the pinning sites in an ordered array corresponding to the spacing of the flux line lattice. (Matsumoto *et al*, 1993, Zhou *et al*, 1993)

The goal of our project is to engineer a multilayer thin film to maximize the pinning characteristics of the NbTi two-phase microstructure. An artificial microstructure made of thin multilayers of α-Ti and NbTi alloy would model the flux pinning microstructures of the conventional NbTi alloy. Ideally, this modeling would further the understanding of flux pinning mechanisms, and provide information on how to optimize the J_c of NbTi and other systems.

In the first phase of the project, several multilayers of alternating Niobium and Titanium were made by DC Magnetron Sputtering onto Silicon substrates. The thickness of the layers was designed to be similar to the spacing of the FFL at 6 Tesla. Samples of the single elements were also fabricated to test for Oxygen contamination, and to test the crystal order obtainable using the sputtering technique. Table 1 lists the basic structural properties of niobium and titanium. Niobium is a Type II superconductor with T_c = 9.3 K. Titanium is a Type I superconductor with T_c = 0.4 K.

Table 1. Niobium and Titanium Material Characteristics

Element	Atomic Number	Atomic Structure	Lattice Parameter	Lattice Spacing	Density
Nb	41	bcc	3.299 Å	(110) 2.334 Å	8.55 g/cm^3
Ti	22	hcp bcc	a = 2.951 Å c = 4.684 Å 3.307 Å	(0001) 2.342 Å (110) 2.355 Å	4.54 g/cm^3

The NbTi multilayers were designed to have an overall composition of 47 weight percent titanium. This composition was chosen for its high values of critical temperature (T_c = 9.1 K), upper critical field ($H_{c2} \cong$ 11.5 Tesla), and critical current density (J_c 2000 Amps/mm2 at 4.2 K and 5 Tesla).

Initial electrical characterization of our NbTi multilayer shows that it does not exhibit superconducting behavior above 4.2 K. There are three possible explanations. First, proximity effect coupling theory suggests that for the geometry of the films created in this project, the averaging of the properties of the two metals will reduce the T_c below 4.2 K. Secondly, oxygen contamination has been known to reduce the T_c of Nb systems.(Koch et al, 1974). Finally, Transmission Electron Microscopy (TEM) shows nano-crystallinity and strain effects that may limit the electronic mean free path. In the case of no oxygen contamination, it was still not clear whether the disorder and limited mean free path in these films adds to the depressed T_c. Figure 1 shows a diagram of the

T_c of NbTi alloys as a function of weight percent titanium. The examples of multilayer specimens tend to have a reduced T_c from the expected bulk alloy value.

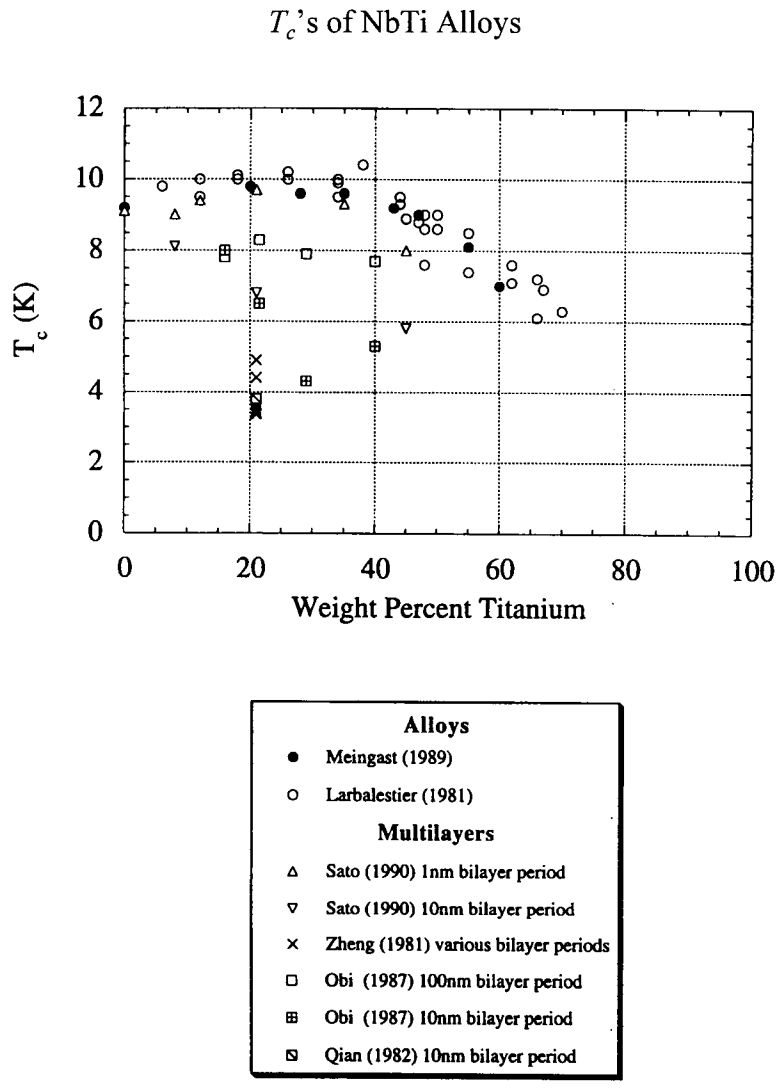

Figure 1. Diagram of T_c for several alloys and multilayers of NbTi as a function of weight percent Titanium.

One way to determine if crystal disorder contributes to the low T_c of the multilayers is to anneal them to induce recrystallization. Amorphous and nano-crystalline metals are not at equilibrium. Any added energy into the system will increase atomic mobility and cause either recrystallization or interdiffusion. Ideally, we wanted the multilayer to recrystallize before interdiffusion destroyed the multilayer and the pinning microstructure. If the multilayer still does not exhibit measurable superconducting properties, further heat treatments to cause partial interdiffusion would be needed.

1.3 Organization of this Thesis

All the work chronicled here is in the attempt to understand the depressed T_c behavior of the initial set of NbTi multilayers. This thesis is structured as follows. In chapter 2, I discuss several relevant aspects of superconductors and multilayers in general. I give a brief literature review and an overview of diffusion theory. I finish the chapter with a detailed derivation of the finite difference approximation I used to model diffusion in the multilayer. In chapter 3, I discuss the experiments and procedures used to characterize the multilayer. In chapter 4, I present the results and discuss their significance. In chapter 5, I have tried to limit what could easily be hundreds of pages to a few more pressing examples of future work to be done on this project.

2. THEORETICAL

2.1 Multilayer Superconductors

2.1.1 Size Parameters of Importance in Superconductors

The bilayer period (Λ), is the length of the compositional modulation in the multilayer. See figure 2. The bilayer period is dependent on the rate of deposition from the sources being sputtered to make the multilayer. The deposition rates can be adjusted to deliver thickness ratios of the two components that will produce any desired overall composition.

Figure 2. The bilayer period (Λ) is the length of the compositional modulation in the multilayer. It is also the sum of the normal layer thickness, d_N, and the superconducting layer thickness, d_{SC}.

As the individual superconducting layers of the multilayer approach the size of λ, the superconductor can no longer exclude magnetic flux. The intrusion of magnetic flux into the superconductor decouples the electron pair correlation responsible for superconductivity.

2.1.2 Electron Transport

The resistivity of the multilayer, ρ, and the residual resistivity ratio, RRR, can be used to characterize the quality of the deposited multilayer. Scattering of electrons in the multilayer depends not only on the disorder within the layers, but on the interface between the layers. Electrical resistivity has been studied as a function of bilayer period for several types of multilayers. (Zheng *et al*, 1981., Werner *et al*, 1982., Carcia and Suna, 1983.) The resistivity has been shown to increase with decreasing bilayer period. Even in near epitaxially grown NbTa multilayers, the mean free path (MFP) for electron transport is limited by the layer spacing. (Broussard, 1986) Gurvitch has put forward a theory that relates the resistivity of a multilayer at room temperature and at low temperature to that of the MFP in the individual layers. (Gurvitch, 1986) Unfortunately, the theory requires a RRR > 1 in order to calculate the MFPs. The point is made, however, that the MFP is limited not by the layer impurity, but by the individual layer spacing, and that the MFP is typically one half to one quarter of the layer thickness.

2.1.3 Proximity Effect Coupling

The critical temperature of a superconductor of known composition is a direct indication of the quality of the material. Oxygen or other impurities can reduce the T_c. However, the electrical connection of a superconductor and a normal metal will also affect the T_c at the interface. When the interface is a significant proportion of the system, the overall T_c can be significantly degraded.

The work of de Gennes (1964), Werthamer (1963), and Silvert (1975) are a common starting ground for proximity theory. Their theories have been modified most notably by Ledvij *et al* (1988), Sato (1990), and Radovic′ *et al* (1991) for applications to multilayers superconductors.

In theory, the electron pair coupling responsible for superconductivity extends a short distance into any normal metal in contact with the superconductor. However, the coupling is also weakened just inside of the superconductor. The multilayer theories attempt to predict the depression of T_c for the multilayer as a function of bilayer period (Λ). Experimentally, the bilayer sizes of multilayers may be separated into three distinct regions, as shown in figure 3.

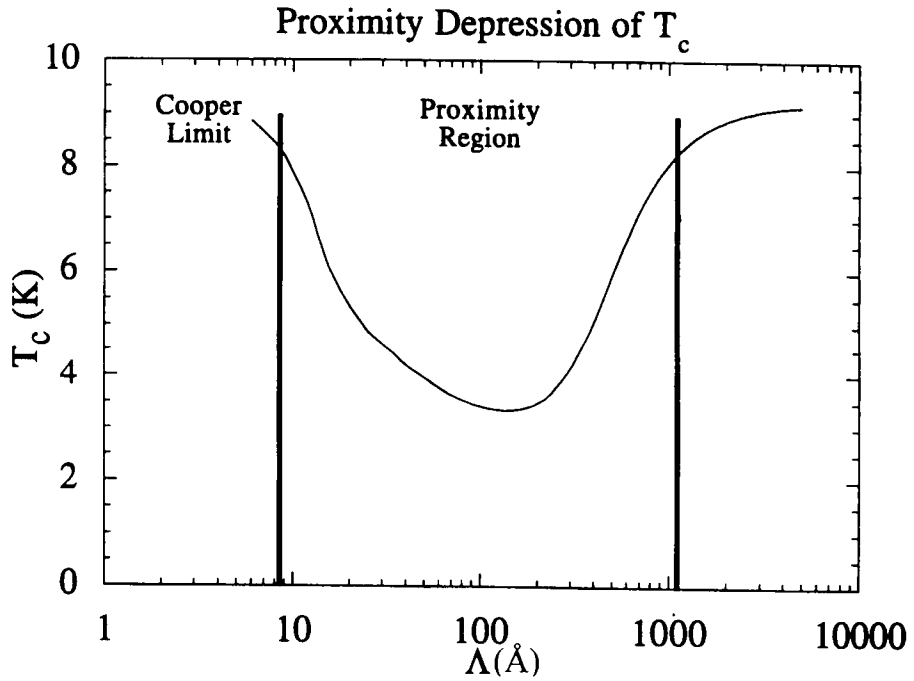

Figure 3. The T_c characteristics of the three regions of bilayer period size.

In the first region, called the Cooper limit (Cooper, 1961), the bilayer period is smaller than the coherence length of the bulk superconductor. The T_c of this system approaches the T_c of the bulk alloy of the overall composition of the multilayer system.

In the second region, as the bilayer period increases and approaches the size of ξ_o, there is a depression of T_c due to the averaging of the superconducting order parameters in the superconducting and normal layers. This region is defined as the proximity effect region.

In the third region, at bilayer periods $\Lambda \gg \xi_o$, the T_c recovers to that of the individual superconducting layers, in our case, the niobium.

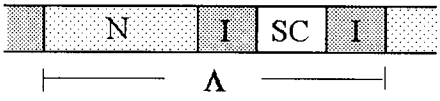

Figure 4. The trilayer period incorporates an interlayer which is an alloy of the normal and superconducting metals.

Each of these regions has been successfully described by theory separately. Theory has been less useful in describing the three regions simultaneously. Ledvij *et al* (1988) approach proximity effect using a trilayer model,

$$\Lambda = d_S + d_N + 2d_I, \qquad [2.1]$$

as shown in figure 4. The interlayer region (I) of thickness d_I, is formed due to interfacial roughness created during deposition, or due to an alloy created by interdiffusion. The Ledvij *et al* solutions for T_c are very complex, and their derivation is beyond the scope of

this thesis. Using the Gor'kov equations of superconductivity, Ledvij *et al* find solutions to the T_c of the multilayer system as a function of Λ. The solutions include several free parameters, including d_I, the layer coherence lengths, $\xi_{S,N,I}$, and electron scattering strengths by fitting the experimental study of T_c versus bilayer period of pure Nb/Ti multilayer films reported by Qian *et al* (1982). By using appropriate input parameters, the Ledvij *et al* model can be used to predict the upper critical field (H_{c2}) as a function of tri-layer period at a given temperature. The T_c can then be calculated for an H_{c2} of zero.

2.1.4 Literature Review of Previous Multilayer Work

Several studies of Nb-Ti multilayers have been conducted in the last decade. Sato (1990) made multilayers of Nb and Ti with various thickness ratios and with various bilayer periods. He deposited the films using DC magnetron sputtering in Argon and mixed Argon and Nitrogen atmospheres. He reports that the T_c's were depressed due to proximity coupling. He indicates that the thin films were thermally stable up to 500°C based on anneals from 200°C to 600°C for 1 hour. He indicates that there was still evidence of a layered structure for the 600°C annealed sample as evidenced by low angle diffraction peaks. He also indicates that X-ray peak shifts occurred for the 400°-600°C anneals due to atomic mobility and diffusion. He works through a partial derivation of proximity effect to explain the depressed T_c's.

Qian *et al* (1982) report T_c and upper critical field parallel to the current flow ($H_{c2//}$) of equal layer thickness multilayers of Nb and Ti from 6 to 6250Å bilayer periods.

Zheng *et al* (1981) made a series of small bilayer period multilayers of Nb and Ti. They report room temperature resistivity and T_c as a function of bilayer period. An *et al* (1986) conducted low temperature interdiffusion in multilayers of Nb-Ti at 300°C and 350°C for times ranging upwards of 3 days. They measured the diffraction peak intensity decay due to reordering and diffusion as a function of time to determine the mutual interdiffusivity ($\tilde{D}$). Their values for $\tilde{D}$ match extrapolated high temperature results from other work.

2.2 Diffusion Theory

Binary diffusion has been the subject of study for over a century. Crank (1975) has devoted an entire text to numerical solutions of partial differential equations for diffusion in various mediums and with various boundary conditions. The standard equation for diffusion is Fick's Second Law

$$\frac{\partial c}{\partial t} = \frac{\partial}{\partial x}\left(\tilde{D}\frac{\partial c}{\partial x}\right) \qquad [2.2]$$

where c is the concentration and $\tilde{D}$ is the mutual interdiffusion coefficient, which is a function of temperature and usually of concentration. When the diffusion coefficient is not a function of composition, Grube's solution is the generally accepted solution (Carter, 1979),

$$\frac{C_{x_1} - C_{x_2}}{C_{x_1} - C_0} = erf\left(\frac{x_2 - x_1}{2\sqrt{\tilde{D}t}}\right) \qquad [2.3]$$

where C_{x_1} is the concentration at some point x_1 meters from the original interface, C_{x_2} is the concentration at some point x_2 meters from the same interface, x_2 - x_1 is the distance between the two points. The error function is the statistical function given by

$$erf(y) = \frac{2}{\sqrt{\pi}} \int_0^y e^{-y^2} dy \qquad [2.4]$$

This solution works well for most systems where the $\tilde{D}$ is not a strong function of composition and is known. However, complications arise when there are periodic boundary conditions, such as those in a multilayer, when there is initially a steep concentration gradient, or when the intrinsic diffusivities vary over several orders of magnitude. All of these limitations come into play in our multilayer systems.

Cook and Hilliard (1969) postulated a fourth order differential equation

$$\dot{c} = \frac{\tilde{D}}{d^2}\left[\nabla^2 c - \left(\frac{2K}{f''_{(c)}}\right)\nabla^4 c\right] \qquad [2.5]$$

to account for the steep concentration gradients in binary diffusion couples. The interatomic spacing is given by d; K is the gradient energy coefficient, and $f''_{(c)}$ is the second derivative of the Helmholtz free energy with respect to composition. Since this equation incorporates thermodynamic data which is not readily available for Nb/Ti binary diffusion couples, this treatment is best suited to measuring these quantities after diffusion has occurred. In addition, $\tilde{D}$ in this treatment is a constant. The intrinsic diffusivities of Nb and Ti, and therefore $\tilde{D}_{NbTi}$ are strong functions of composition.

The diffusion modeling in this thesis uses measured values of the intrinsic diffusivities of Nb and Ti through alloys of NbTi as a function of the Nb concentration.

(Gibbs *et al*, 1963, Pontau and Lazarus, 1979, Moffat, 1985) A finite difference approximation is used to predict the amount of interdiffusion that would occur for a given heat treatment. The Nb/Ti multilayers were annealed and microstructurally and electromagnetically characterized to compare with the interdiffusion predicted by the computer diffusion model.

2.3 Derivation of Finite Difference Approximation of Fick's Second Law

An explicit finite difference approach is used to model the time dependent composition of a multilayer Nb and Ti thin film during annealing. The geometry of the multilayer thin film can be modeled as one dimensional of periodic composition.

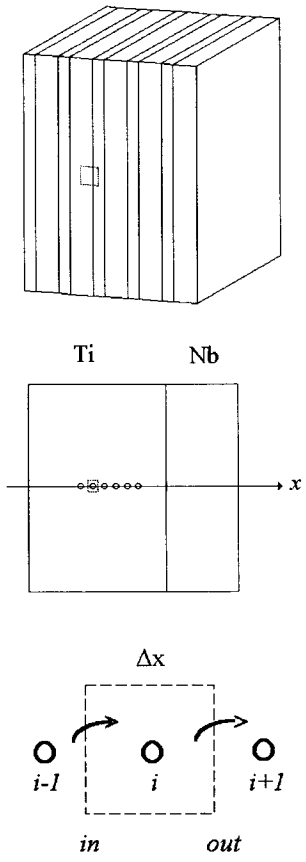

Figure 5. The control volume around a finite element node, with height and depth of unity, used to derive Fick's Second Law for diffusion in one dimension.

Beginning with the control volume shown in figure 5, the mass accumulation at node i is equal to the amount of flux into the control volume (around node i) minus the flux out of the control volume, during the time increment. Written in finite difference form,

$$\Delta x\left(c_{i,t+\Delta t} - c_{i,t}\right) = \left[\left(-D(c_{in})\frac{\partial c}{\partial x}\right)_{in}\Delta t - \left(-D(c_{out})\frac{\partial c}{\partial x}\right)_{out}\Delta t\right] \qquad [2.6]$$

The control volume here has a height and depth of one, and all concentration gradients are assumed to vary in the x direction only. Rearranging equation [2.6] yields

$$\frac{\left(c_{i,t+\Delta t}-c_{i,t}\right)}{\Delta t}=\frac{\left(D(c_{out})\frac{\partial c}{\partial x}\right)_{out}-\left(D(c_{in})\frac{\partial c}{\partial x}\right)_{in}}{\Delta x} \qquad [2.7]$$

This is equivalent to the partial differential equation,

$$\frac{\partial c}{\partial t}=\frac{\partial}{\partial x}\left(D(c)\frac{\partial c}{\partial x}\right) \qquad [2.8]$$

which is Fick's Second law for diffusion, including the compositionally dependent diffusivities, $D(c)$. Further simplification of equation [2.7], using the notation

$$D_i = D(c_i),\ D(c_{in})=\frac{D_{i-1}+D_i}{2}, \text{ and } D(c_{out})=\frac{D_i+D_{i+1}}{2},$$

yields

$$\frac{\left(c_{i,t+\Delta t}-c_{i,t}\right)}{\Delta t}=\frac{\left(\frac{D_i+D_{i+1}}{2}\right)\left(\frac{c_{i+1,t}-c_{i,t}}{\Delta x}\right)-\left(\frac{D_{i-1}+D_i}{2}\right)\left(\frac{c_{i,t}-c_{i-1,t}}{\Delta x}\right)}{\Delta x} \qquad [2.9]$$

and

$$c_{i,t+\Delta t}=c_{i,t}+\frac{\Delta t}{2\Delta x^2}\left[\left(D_{i+1}+D_i\right)\left(c_{i+1,t}-c_{i,t}\right)-\left(D_{i-1}+D_i\right)\left(c_{i,t}-c_{i-1,t}\right)\right] \qquad [2.10]$$

Collecting terms yields,

$$\begin{aligned} c_{i,t+\Delta t} &= c_{i-1,t}\left[\frac{\Delta t}{2\Delta x^2}\left(D_{i-1}+D_i\right)\right] \\ &+ c_{i,t}\left[1-\frac{\Delta t}{2\Delta x^2}\left(D_{i-1}+2D_i+D_{i+1}\right)\right] \\ &+ c_{i+1,t}\left[\frac{\Delta t}{2\Delta x^2}\left(D_i+D_{i+1}\right)\right] \end{aligned} \qquad [2.11]$$

Exponential fits to the prefactors (D_o) and activation energies (Q) of Nb and Ti obtained from Gibbs *et al*, yield

$$D_o^{Nb}=5.5783\times10^{-4}\exp\left(8.209\times f_{Nb}\right)\frac{\text{cm}^2}{s} \qquad [2.12]$$

$$Q_{Nb} = 31463 + (65740 \times f_{Nb}) \frac{\text{cal}}{\text{mol}} \quad [2.13]$$

$$D_o^{Ti} = 1.663 \times 10^{-3} \exp(2.299 \times f_{Nb}) \frac{\text{cm}^2}{s} \quad [2.14]$$

$$Q_{Ti} = 33991 + (54400 \times f_{Nb}) \frac{\text{cal}}{\text{mol}} \quad [2.15]$$

where f_{Nb} is the atomic fraction of Nb in the NbTi alloy. The intrinsic diffusion coefficients are determined from

$$D = D_o \exp\left(\frac{-Q}{RT}\right) \quad [2.16]$$

where T is the temperature, in Kelvin.

In the computer code written to model the interdiffusion of the multilayer, the concentration of each element is solved at each node simultaneously. A stability criterion, limited by the node spacing Δx, the time increment Δt, and the fastest compositionally dependent intrinsic diffusion coefficient, $D_{Nb}(c_{Nb} = 0)$ is maintained to allow the solution to converge. The calculations were conducted on a SPARC 20 workstation. The program code is included in the Appendix.

I theorized that reordering should occur at some low temperature before macroscopic interdiffusion destroyed the multilayer. I reasoned that if enough energy was put into the system to cause interdiffusion only within the first monolayer or two of the interface, there should also be enough energy for disordered atoms inside the layers to locally rearrange to more stable configurations. After reordering, if the multilayer still did not exhibit superconducting properties above 4.2 K, then proximity effect coupling

was the main cause of the depressed T_c's. Further heat treatments would be done to cause increasing interdiffusion, while still maintaining a modulated composition. The resulting diffusion profiles could be analyzed to determine the interlayer thickness and multilayer degradation predicted by the diffusion model and compared to microstructural measurements.

3. EXPERIMENTAL PROCEDURE

3.1 Multilayer Sample Fabrication

Samples were made at Lawrence Livermore National Laboratory using a multiple target DC Magnetron Sputtering system. Two Torus 10 magnetrons were mounted in an upright position. The substrates rest on a platen which allows the substrate to face downward toward the source. The platen is driven in a planetary motion by a high precision stepper motor. A Hewlett Packard HP9133 monitors the deposition rate and records the platen rotational velocity by a precision shaft encoder. The system was evacuated below 10^{-7} torr prior to initiating sputtering.

Multilayers are made by rotating the platen holding the samples over the sources. Shields around the sources prevent mixing of the plasmas. The first set of depositions was conducted at ambient temperature, and never exceeded 115°C. The process gas was 99.995% pure Argon at a pressure of 3 millitorr. A second set of pure films was made at 200°C with 5 millitorr of Argon pressure. The substrates are 4 inch, <100> p-type silicon wafers. Residual gas analysis of the system prior to deposition showed negligible oxygen in the system.

Table 2 details the films made to date. Sample set NbTi 4003 was the focus of this thesis.

Table 2. Information pertaining to what multilayers were made.

Sample Number	Sample Chemistry	Reported Layer Thickness by LLNL (nm)	Number of Bilayers	Measured Bilayer Period (nm)	Reported Total Thickness (μm)
4001	Nb/Nb	17.8 / 17.8	63	-	2.23
4002	Ti/Ti	10.7 / 10.7	150	-	3.2
4003	**Nb/Ti**	**6.1 / 10.7**	**120**	**13.6 (XRD)**	**2.0**

Samples deposited with 5 millitorr Ar Gas Pressure and 200° C Deposition

4004	Nb/Nb	17.1 / 17.1	140	-	4.8
4005 Ti Buffer Layer	Nb/Nb	17.1 / 17.1	140	-	4.8

3.2 Heat Treatments

An initial heat treatment was conducted at 300°C in order to determine whether disorder and reduced electronic mean free path contributes to the depression of T_c in the multilayer. After determining that recrystallization had indeed occurred, and that the multilayer still did not exhibit superconducting properties above 4.2 K, further heat treatments were conducted to interdiffuse the Nb and Ti to form a larger interlayer. All heat treatments were chosen based on the profiles obtained from the computer diffusion model.

Samples from NbTi #4003 and NbNb #4001 were wrapped separately in cold rolled Nb foil and put into Pyrex tubes. A wad of Nb foil was added at one end of the tubes as a sacrificial oxygen getter. The tubes were evacuated to 50 millitorr using a mechanical roughing pump. The tubes were then evacuated to 10 millitorr using a diffusion pump. Each tube was flushed 5 times with high purity Argon gas and pumped down to 10 millitorr between flushes to reduce the partial pressure of oxygen. After the final Argon flush, the tubes were evacuated to 10 millitorr for over one hour.

The tubes were sealed with a 3600°C torch using MAPP gas. The vacuum in the sealed tube was checked by heating the tube wall around the sacrificial Nb foil wad. This served two purposes. One, the heating of the Nb foil wad would getter any oxygen still remaining in the tube. Two, when the tube wall became hot enough, the wall began to collapse due to the vacuum inside the tube. This confirmed the tube still maintained a vacuum after sealing. One Pyrex tube cracked during a heat treatment at 400°C. The Nb foil wraps and wad were heavily oxidized. All other samples came out clean and ductile with no signs of oxidation.

The heat treatment schedule between 300 and 600°C conducted on the NbTi 4003 samples is detailed in Table 3. The heat treatment of 600°C was performed to completely interdiffuse the multilayer structure to test for the bulk superconducting properties of homogeneous $Nb47^{w}/_{o}Ti$.

Table 3. Heat Treatment Schedule of NbTi 4003 Multilayers

Temperature	Time
300°C	1,3,& 10 hours
400°C	1,3, & 10 hours
450°C	1,3, & 10 hours
600°C	1 hour

3.3 Characterization of Properties

3.3.1 X-ray Diffraction

Bragg diffraction occurs when X-rays are elastically scattered by periodic arrays of electrons. As shown in figure 6, constructive diffraction occurs for any array spacing d, given by Bragg's law

$$n\lambda = 2d\sin\theta \qquad [3.1]$$

where n is the order of diffraction, λ is the incident X-ray wavelength, θ is the Bragg angle, and d is the modulation spacing. The modulation spacing can be due to adjacent atomic planes or the compositional spacing of a superlattice, as in a multilayer.

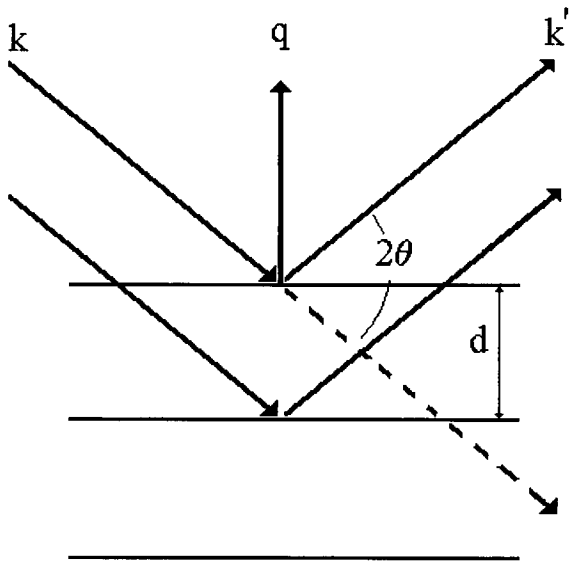

Figure 6. Bragg Diffraction of X-rays.

X-ray diffraction was conducted on a Seimens Diffraktometer Model D5000 located in the Chemistry Department of Oregon State University. High and low angle 2θ scans were conducted on all samples before and after heat treatments. The divergence and antiscatter slits were programmed to irradiate a 6 mm sample length, independent of θ. Cu $K\alpha_1$ radiation with a wavelength of 1.5406 Å was used to irradiate the samples. Low angle scans were conducted to determine the bilayer period before and after anneal.

The bilayer period, Λ, of the multilayer is determined from the modified Bragg equation

$$m\lambda = 2\Lambda \sin\theta\left(1 - \frac{2\delta}{\sin^2\theta}\right)^{1/2} \qquad [3.2]$$

where λ is the radiation wavelength, θ is the measured low angle diffraction peaks, in radians. The average deviation of the diffraction index from unity, δ, represents the imperfect nature of the crytal lattice as it differs from perfect Bragg diffraction. It is typically on the order of 10^{-5}. (Slaughter *et al*, 1994) By fitting the measured low angle diffraction peaks to equation [3.2], the bilayer period and average deviation from unity can be determined. The degradation of peak intensity is a function of the interdiffusion that takes place at the interface.

Measurements of full width at half maximum (FWHM) at high angle were done using the Scherrer formula

$$\text{FWHM} = \frac{0.9\lambda}{t_q \cos\theta} \qquad [3.3]$$

where t_q is the average distance over which phase coherence is maintained. (Broussard, 1986). Because of the two-dimensional geometry of the multilayer, t_q is a measure of the coherence in a direction normal to the multilayer planes.

3.3.2 Tranmission Electron Microscopy

TEM samples were started by cleaving 2-3 mm wide strips from the original substrate. The strips were epoxied together with the multilayer sides facing each other. For mechanical support, 3mm wide strips of aluminum were epoxied on the back of each side of the specimen. This "sandwich" was clamped and baked at 80°C for 30 minutes to harden the epoxy. The sandwich was then sectioned into 300μm thick, transverse cross sections with a low speed diamond cut off saw.

Each sliced cross section was mounted on a high precision hand lapping device with thermal wax. The sample was polished to a mirror finish using a series of polishing papers: 30, 12, 3, 1, 0.25μm. The sample was removed from the hand lapping device, flipped, remounted, and lapped on the other side. The sample was lapped to ~100 μm, ~60 μm, and 50 μm in thickness with the 30, 12, and 3μm polishing papers, respectively. All lapping of the sample was done parallel to the multilayer/substrate interface.

The samples were then dimpled with an E.A. Fishchione Model 2000 dimpler until the thinnest region of the sample is ~5μm thick. After dimpling, the samples were rinsed in acetone to remove any residual thermal wax. The samples were then ion milled [1mA, 7kV, 10° specimen/beam angle] while mounted on a liquid nitrogen cooled stage. During milling, the sample was rotated at variable speeds to maximize the time the ion beam was perpendicular to the multilayer structure to reduce preferential milling of Si, Ti, or Nb.

TEM bright field imaging was conducted to determine the microstructure and multilayer quality of the samples. Selected Area Diffraction (SAD) patterns were also obtained to determine crystal order information.

3.3.3 Resistivity, ρ and Residual Resistivity Ratio, RRR

The electrical resistivity of rectangular samples, cut from the original substrate, was measured using a four point, spring loaded probe. The samples were typically a few millimeters wide and a minimum of 40 mm long. The DC current, supplied by a Keithley

236 Source Measurement Unit, was ramped while the voltage across a 20 mm constant gauge length was measured using a Keithley 182 Sensitive Digital Voltmeter. The current was ramped up and down to insure there were no heating effects. The resistivity, ρ, was determined from the slope of the $V(I)$ curve, (R) and the sample geometry, as given by

$$\rho = \frac{Rtw}{l}, \qquad [3.1]$$

where t is the sample thickness, w is the width, and l is the gauge length.

Resistivity measurements were conducted at room temperature, 77.2 K and 4.2 K. Superconducting samples were driven normal by high magnetic fields before measuring the low temperature resistance. The residual resistivity ratio (RRR) is the ratio of the resistivities at room temperature to 4.2 K.

3.3.4 Critical Temperature T_c

The critical temperatures (T_c) of the samples were measured using an AC susceptometer. The AC susceptometer uses an excitation field generated by a lock-in amplifier and a wire coil to produce an AC voltage in two identical Hall probes. The sample is situated near one hall probe during testing. The difference in the output voltage from the two Hall probes is measured by the two input channels of the lock-in amplifier. The temperature is simultaneously measured using a calibrated Gallium Arsenide resistence thermometer coupled to the sample by a sapphire single crystal. A transition is noted when the sample changes from a normal metal to a superconductor. At the

transition, the superconducting sample exhibits diamagnetic behavior, inducing shielding currents to flow in the plane of the sample. The field produced by these currents induces a voltage offset between the two Hall probes. The T_c is defined by the midpoint of the transition and the transition width.

3.3.5 Upper Critical Field H_{c2}

The upper critical field (H_{c2}.) was measured using the same four point probe described in section 3.3.3. The samples were positioned in the bore of a 9 Tesla, NbTi superconducting solenoid magnet, submerged in pool boiling liquid Helium at 4.2 K.

A constant current is applied through the sample using a Keithley 236 Source Measurement Unit while the voltage across a 20 mm constant gauge length is measured using a Keithley 182 Sensitive Digital Voltmeter. The magnetic field is slowly increased from zero until a resistive transition is found. The H_{c2} is defined by the midpoint of the transition and the transition width.

3.3.6 Critical Current Density J_c

The critical current (I_c) is measured using the same 4-point probe, current source, and voltmeter used in the electrical resistivity measurements described in section 3.3.3. The I_c is based on the superconducting $V(I)$ curve. A DC current is ramped through the sample while monitoring the voltage across the fixed tap length. The I_c is determined where the superconductor begins exhibiting an induced resistive voltage transition of

about 500μV/cm. The sample is positioned symmetrically in the bore of a superconducting magnet immersed in liquid Helium so that the current and magnetic field are at right angles to each other. The I_c can be measured at different applied magnetic field strengths. The J_c is determined from the I_c and the sample geometry.

4. RESULTS and CONCLUSIONS

4.1 Results

4.1.1 Diffusion Profiles and Interlayer Thickness

Figures 7 through 9 show the calculated compositional profile of a single bilayer period of NbTi, centered about a Nb layer, for heat treatments at 300°C, 400°C, and 450°C. Calculations at 600°C predicted complete interdiffusion in less than one hour. The composition is expressed in both atomic and weight percent Nb for purposes of predicting interlayer growth. The node spacing, Δx, was 5Å for all calculations presented here. Node spacings of 1Å were used in the lower temperature calculation as a verification. They show good agreement with the 5Å node spacing. The stability criterion was the main driving force for larger node spacing. Calculations run on the SPARC 20 at 600°C with a node spacing of 1Å required a time increment of 10^{-6} seconds. After one week of calculation, 5 minutes of diffusion time had elapsed. This approach was considered unacceptable. It is appropriate to point out that the bilayer period used in the calculation differs slightly from that of the actual multilayer.

The intrinsic diffusivities of Nb and Ti were modeled using a straight exponential fit to the empirical results obtained by Gibbs *et al* (1963). However, the Gibbs *et al* data has a slight non-linearity at low Nb concentrations. This would result in slower diffusion initially than that modeled in this thesis.

The majority of diffusion predicted by the model occurs in the first hour. This is due solely to the initial steep concentration gradient at the interface between the niobium and titanium.

An interlayer thickness, d_I, was derived from the diffusion profiles by determining the thickness of the region between 40 and 60 weight percent Nb. The criterion was used based on the limitation of the Ledvij *et al* theory of a fixed composition interlayer. The predicted interlayers are listed in table 4.

Table 4. Interlayer thickness predictions based on diffusion model.

	1 hour	3 hours	10 hours
300°C	0.4 Å	0.6 Å	0.6 Å
400°C	1.8 Å	3.9 Å	6.8 Å
450°C	7.5 Å	20 Å	64 Å

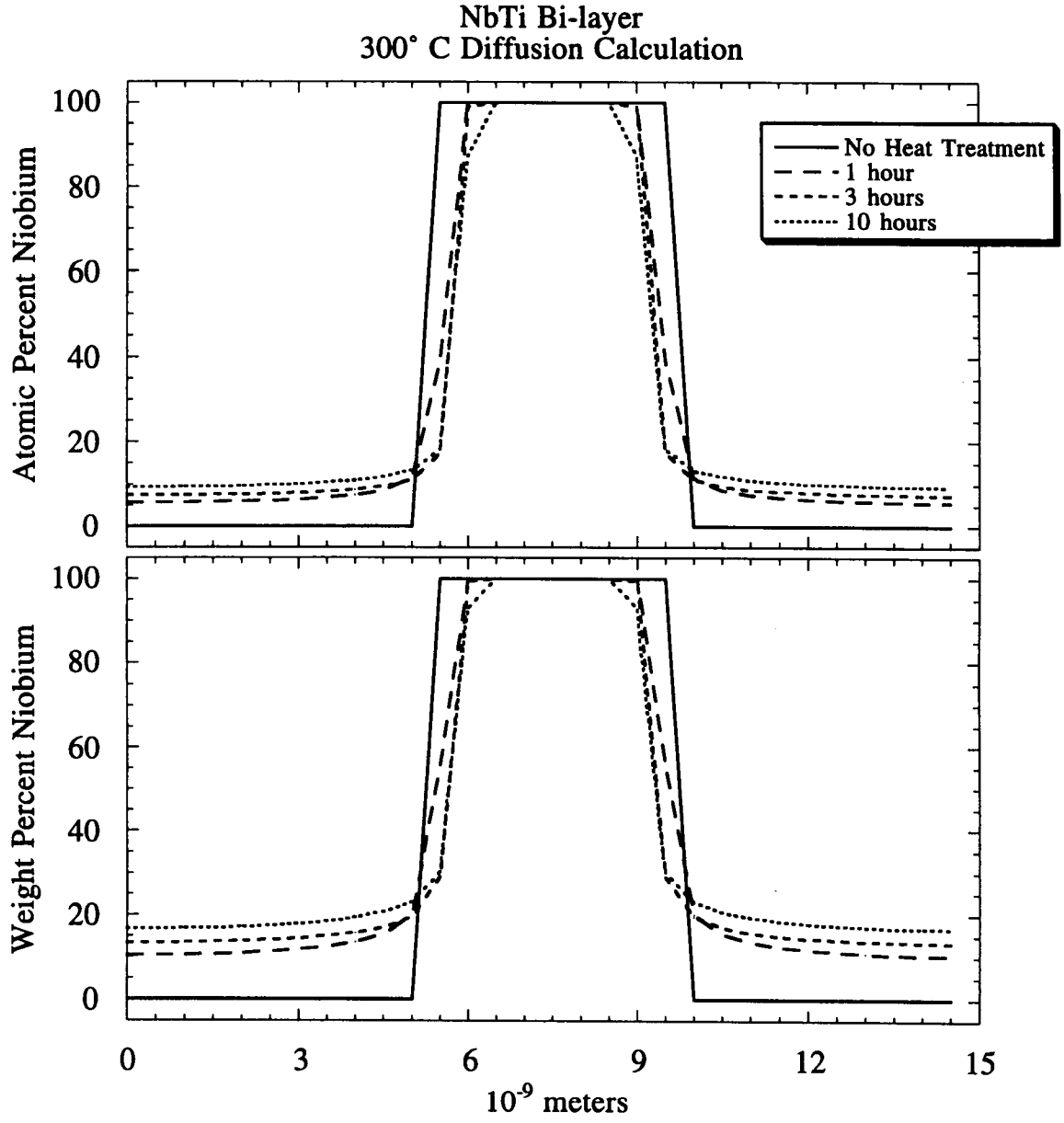

Figure 7. Niobium composition profiles predicted for 300°C for heat treatments of 1,3, and 10 hours.

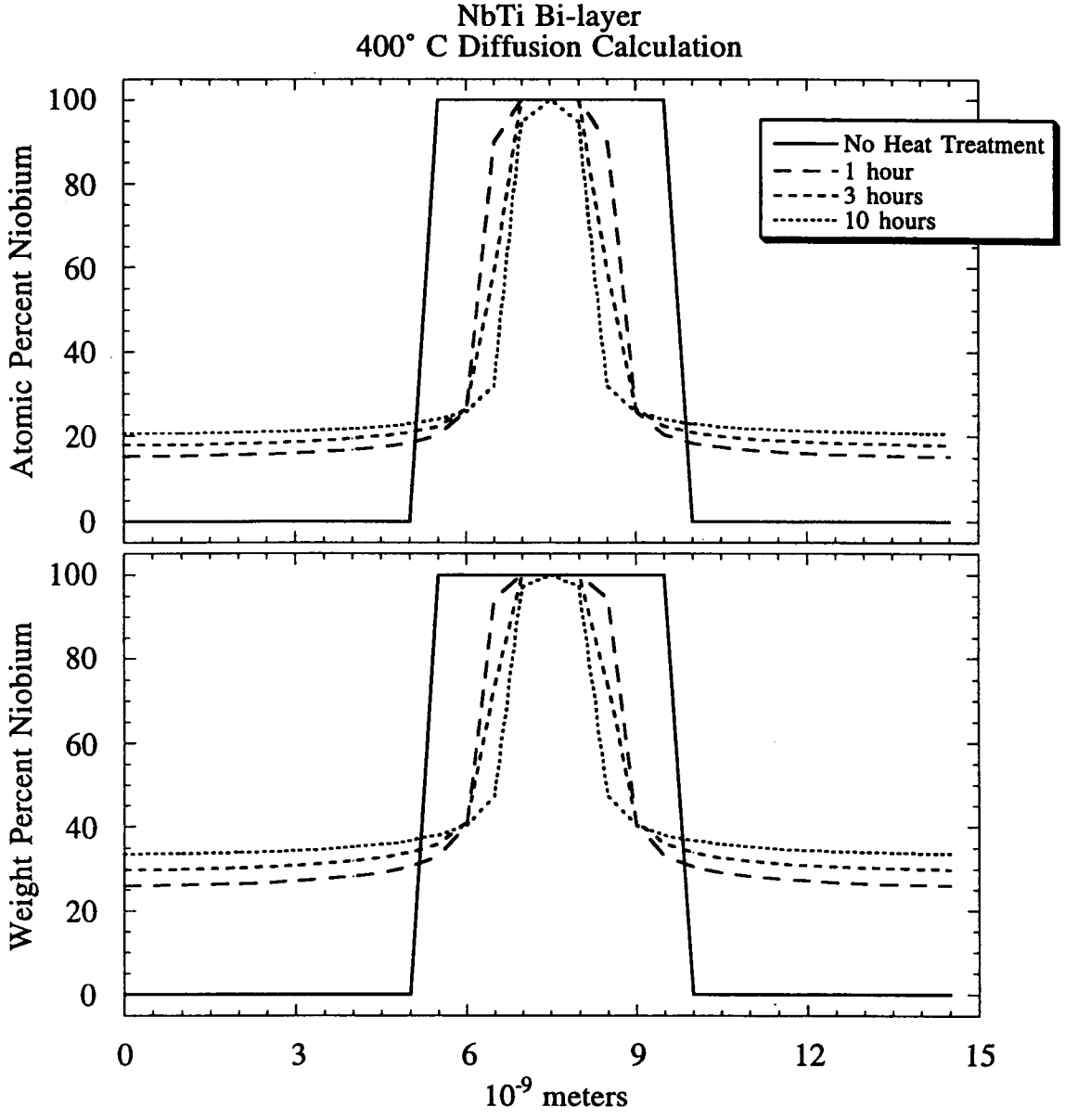

Figure 8. Niobium composition profiles predicted for 400°C for heat treatments of 1,3, and 10 hours.

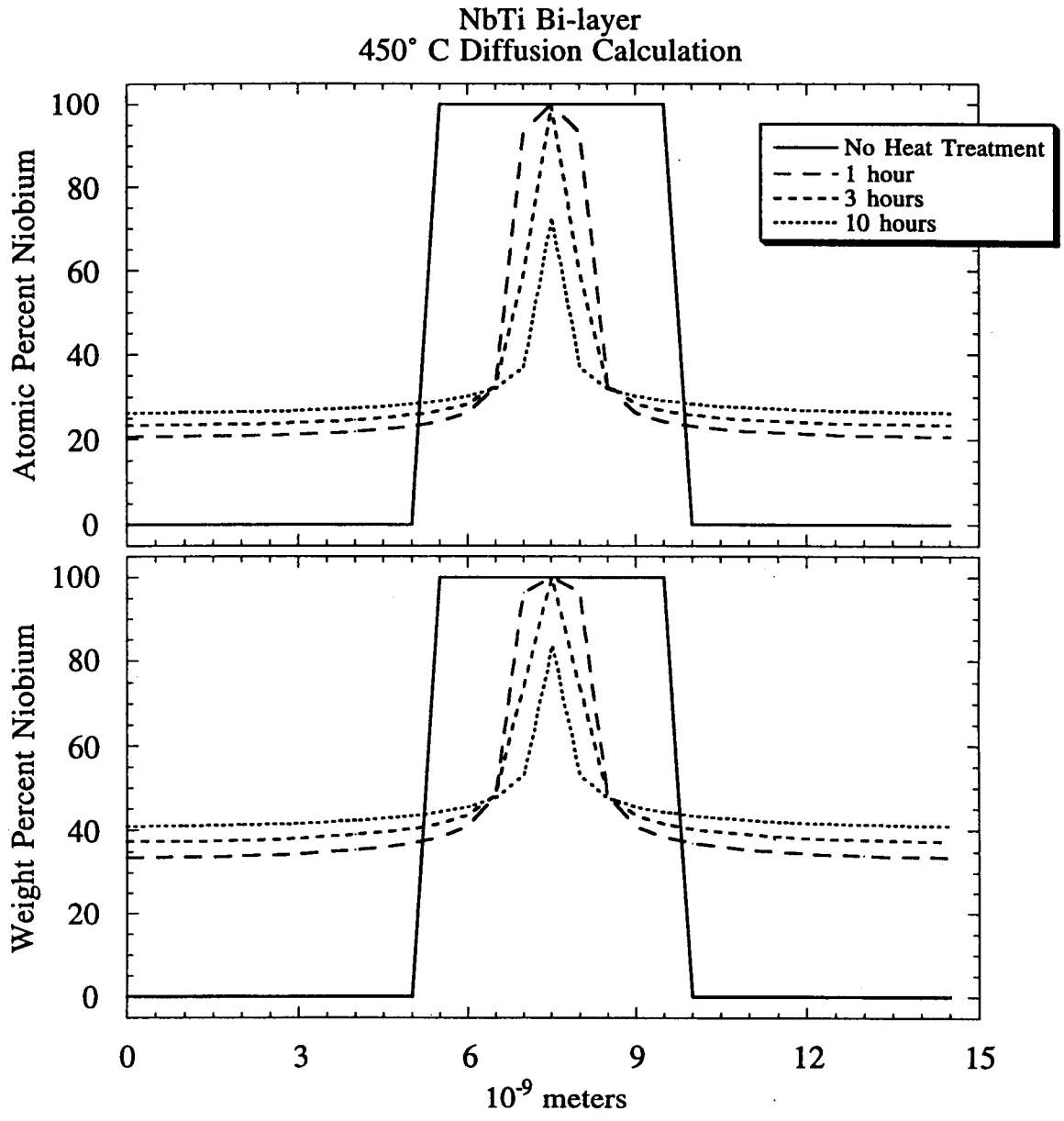

Figure 9. Niobium composition profiles predicted for 450°C for heat treatments of 1, 3, and 10 hours.

4.1.2 X-ray Diffraction

Figures 10 through 13 show the low angle X-ray peaks of the multilayer before and after heat treatment. Excellent layering is evident, even for the sample heat treated at 450°C for 10 hours. The peak heights drop off after a 1 hour anneal for all samples, and remain relatively constant thereafter. The 600°C sample shows no sign of a remaining multilayer structure. The noise at $2\theta < 1°$ is due to detector saturation.

A fit to the no heat treatment sample low angle peaks, shown in figure 14, gives a bilayer period of 135.8Å. This is consistent with measurements taken from TEM, described later.

Table 5 summarizes the FWHM measurements from the high angle diffraction scans.

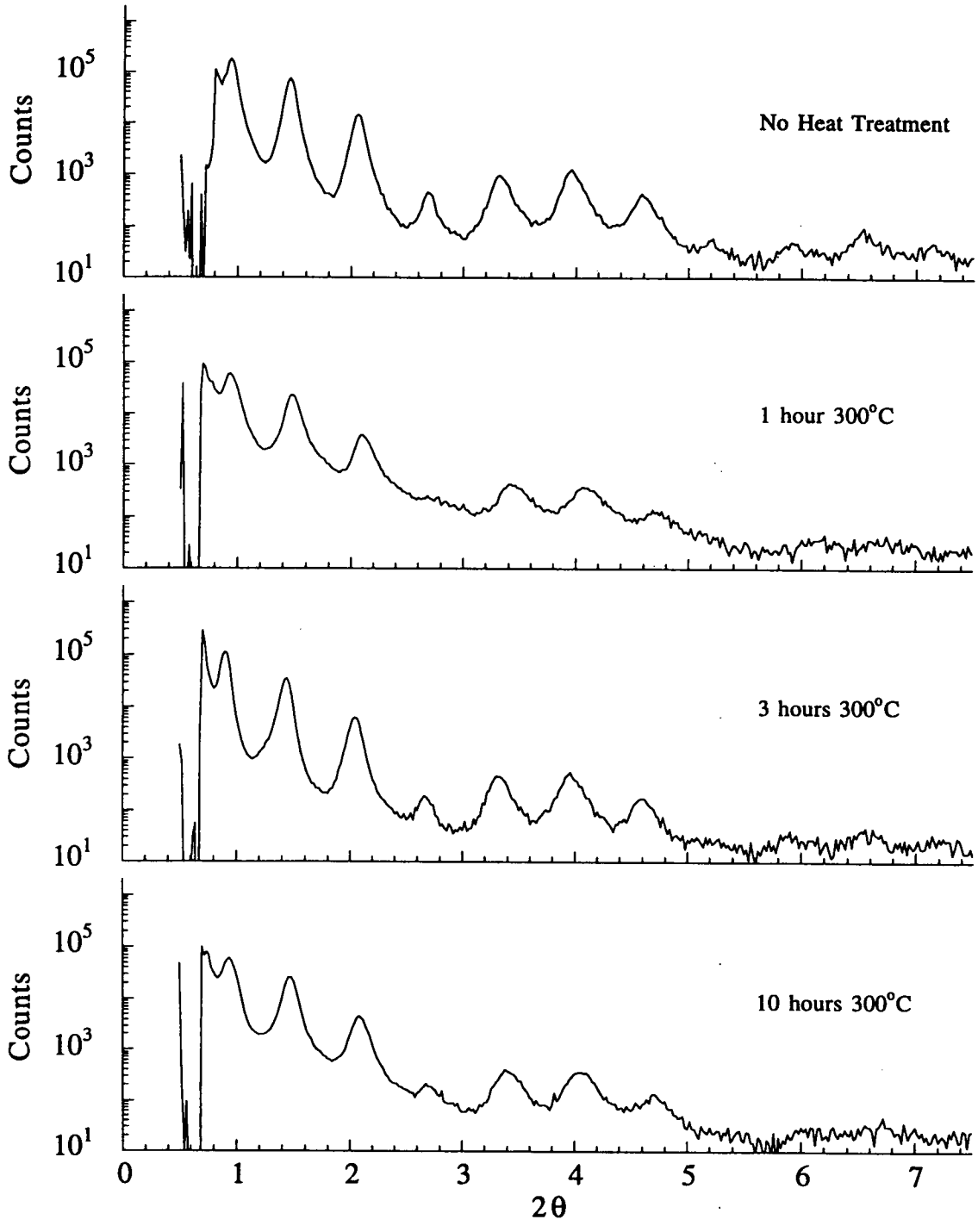

Figure 10. Low angle multilayer peaks before and after heat treatment at 300°C.

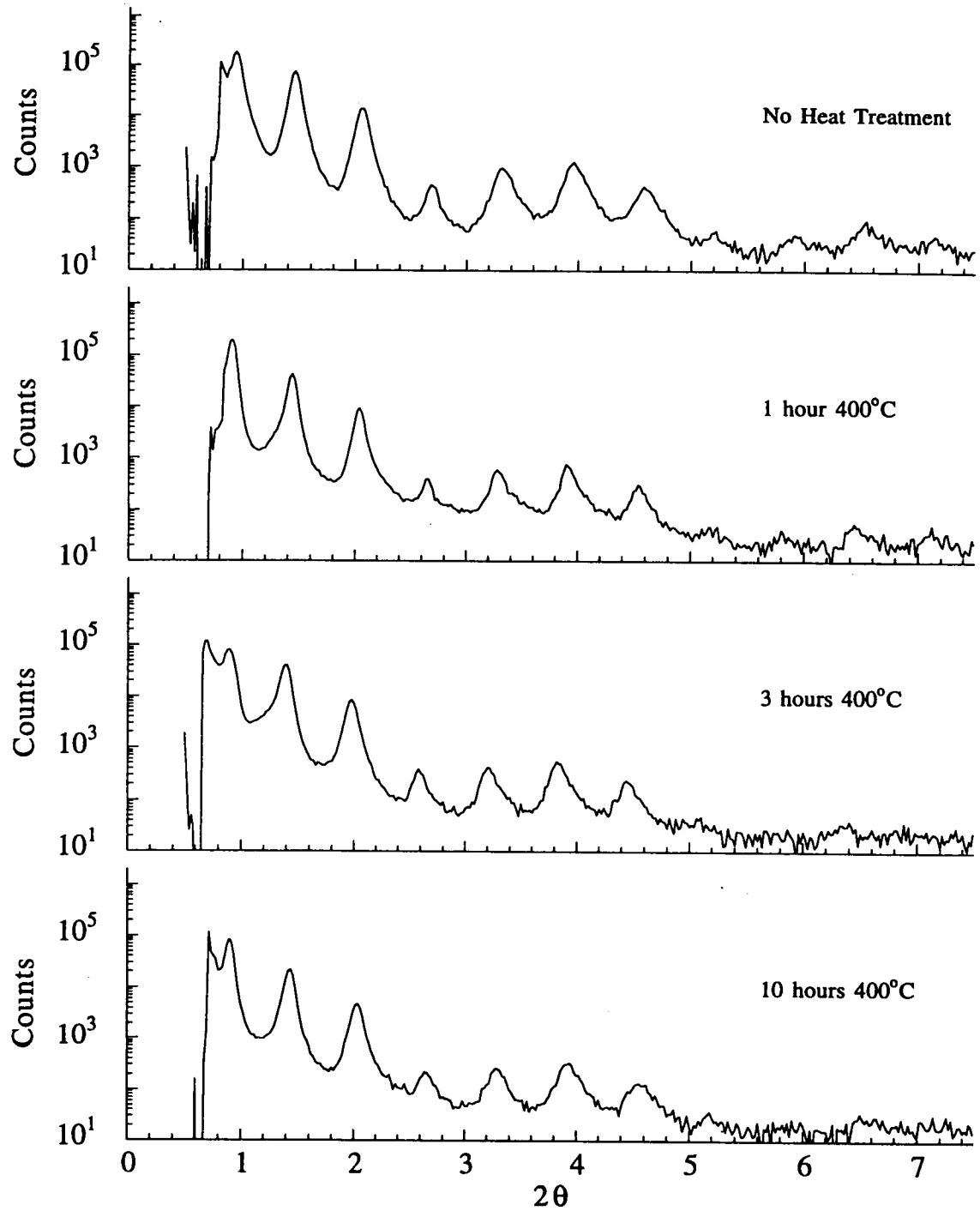

Figure 11. Low angle multilayer peaks before and after heat treatment at 400°C.

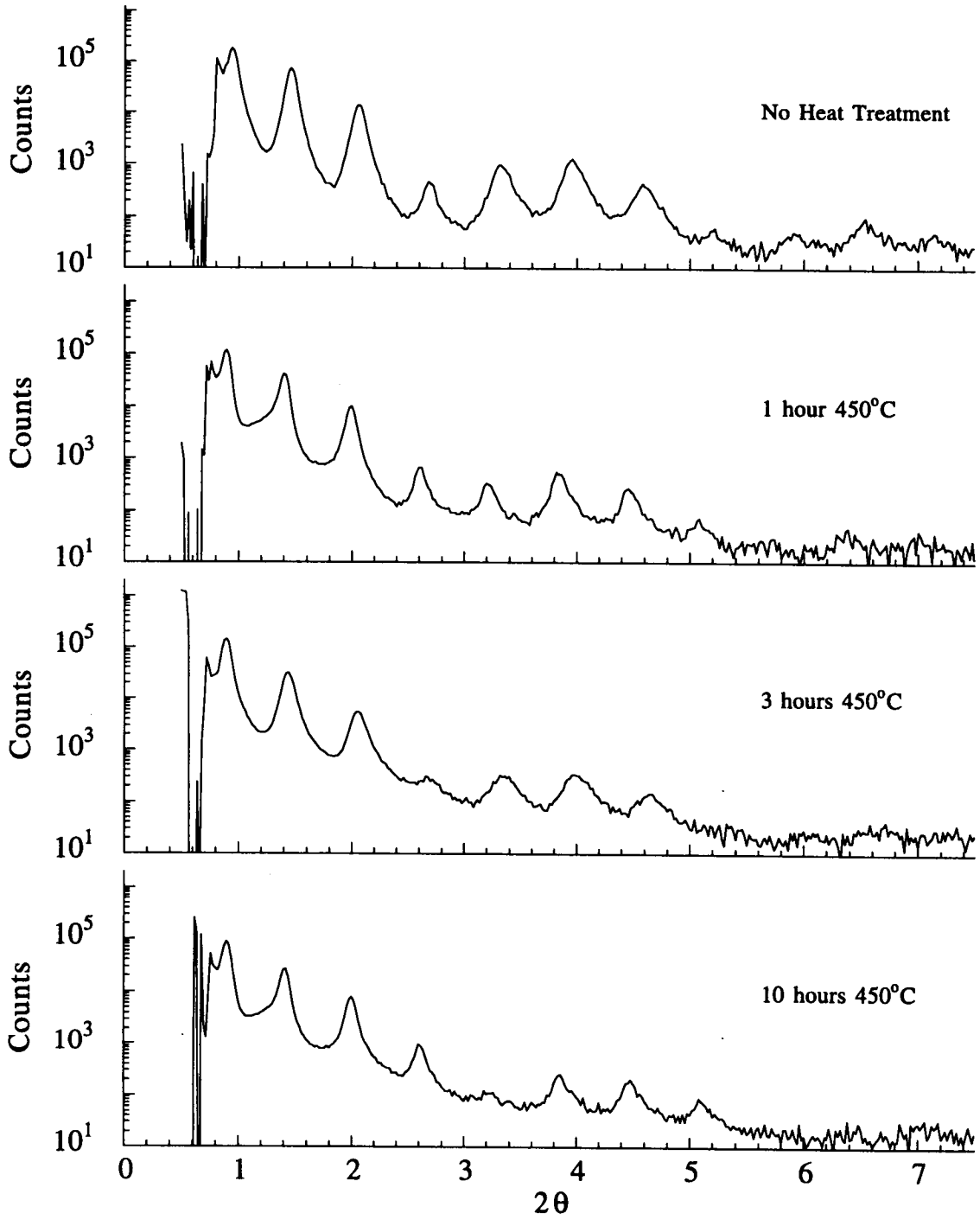

Figure 12. Low angle multilayer peaks before and after heat treatment at 450°C.

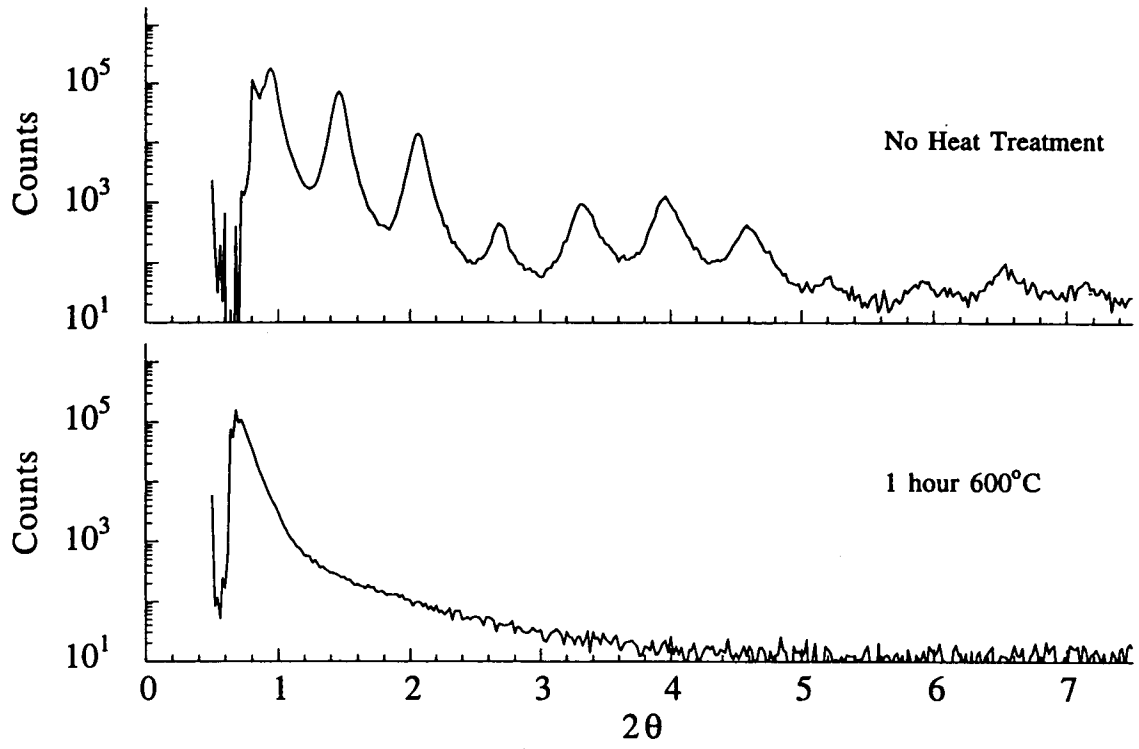

Figure 13. Low angle multilayer peaks before and after heat treatment at 600°C.

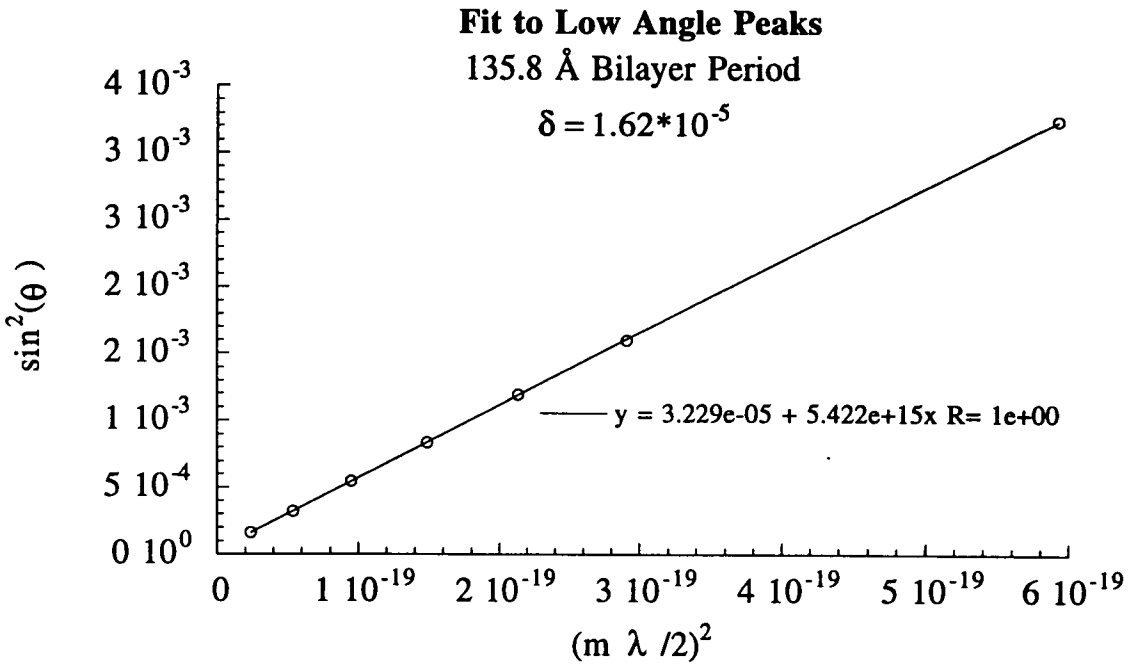

Figure 14. Bilayer period calculation from Low Angle peaks of the No Heat Treatment sample.

Table 5. Summary of FWHM Measurements to determine the average phase coherence.

Sample	110 peak ~ θ = 19.25°	220 peak ~ θ = 41.25°
No Heat Treatment	50 Å	54 Å
1 hour at 300°C	162 Å	88 Å
3 hours at 300°C	153 Å	70 Å
10 hours at 300°C	143 Å	70 Å
1 hour at 400°C	153 Å	78 Å
3 hours at 400°C	162 Å	88 Å
10 hours at 400°C	140 Å	81 Å
1 hour at 450°C	143 Å	106 Å
3 hours at 450°C	200 Å	88 Å
10 hours at 450°C	168 Å	75 Å

4.1.3 TEM

Figures 15 through 20 show TEM cross sections of the NbTi multilayer for various heat treatments. The niobium layers are dark and the titanium layers are light. Clear evidence of the multilayer structure is seen in all images. Layering can be seen to be smooth and uniform with increasing roughness from the substrate to the top of the multilayer. This is due to the columnar growth of the multilayer with a low atomic mobility during deposition (Slaughter *et al*, 1994). The uneven contrast perpendicular to the multilayer is due to the thickness gradient caused during ion milling.

At high heat treatments, the TEM sample preparation became increasingly difficult due to a brittle silicide growth at the multilayer-silicon interface. Based on the resolution of the TEM images, there is a smoothing of the contrast between individual layers. This is evidence for small amounts of interdiffusion. Due to its small scale, no measurements of interlayer thickness can be done from the images. Measurements of bilayer period for the TEM images gives a bilayer of 136Å.

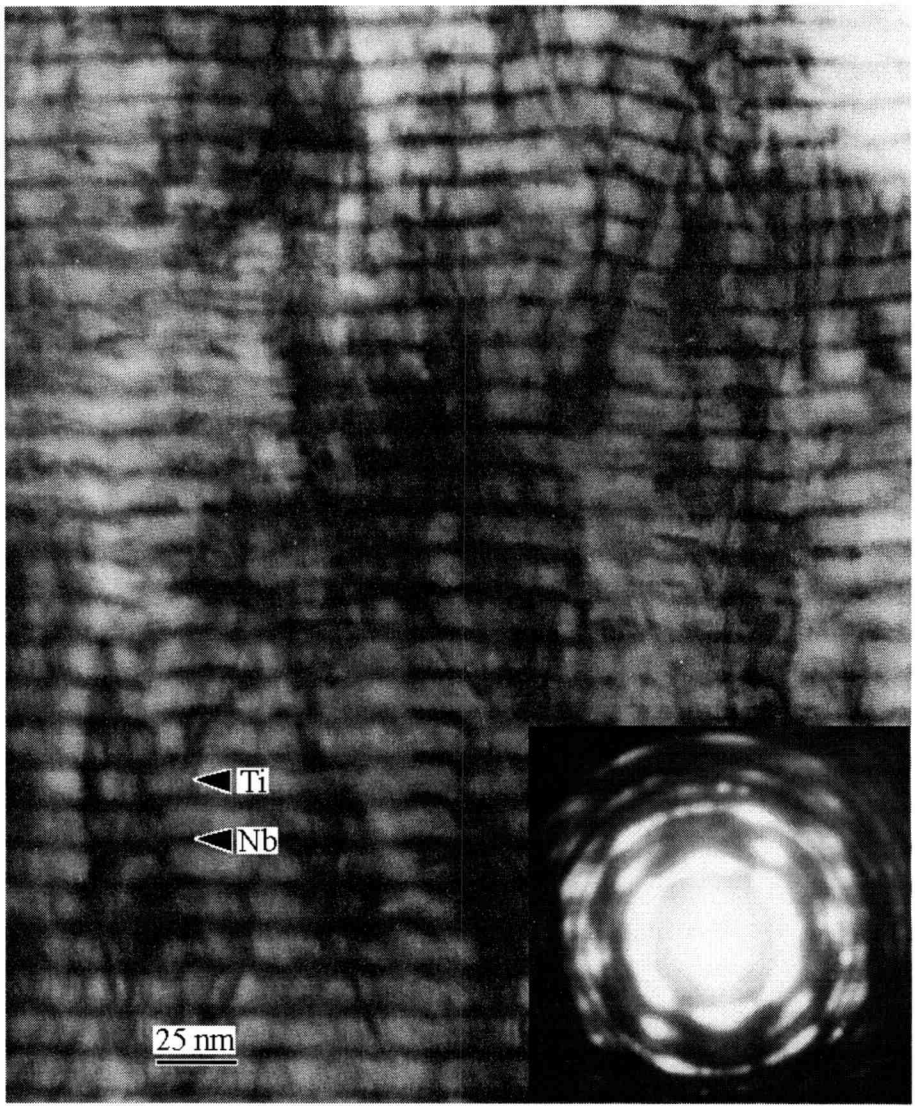

Figure 15. TEM Cross section and SAD of NbTi multilayer before heat treatment.

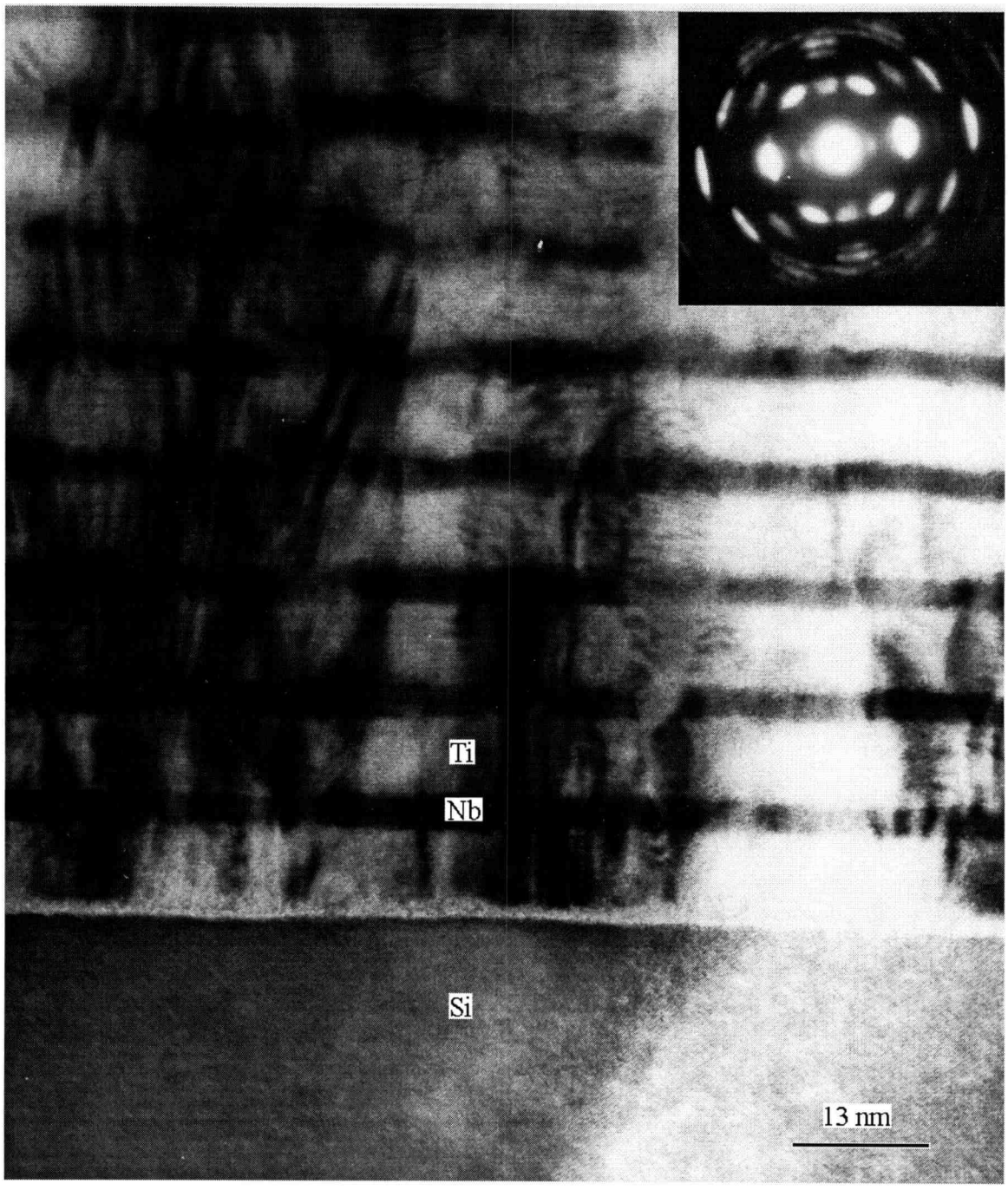

Figure 16. TEM Cross section and SAD of NbTi multilayer after 1 hour at 300°C.

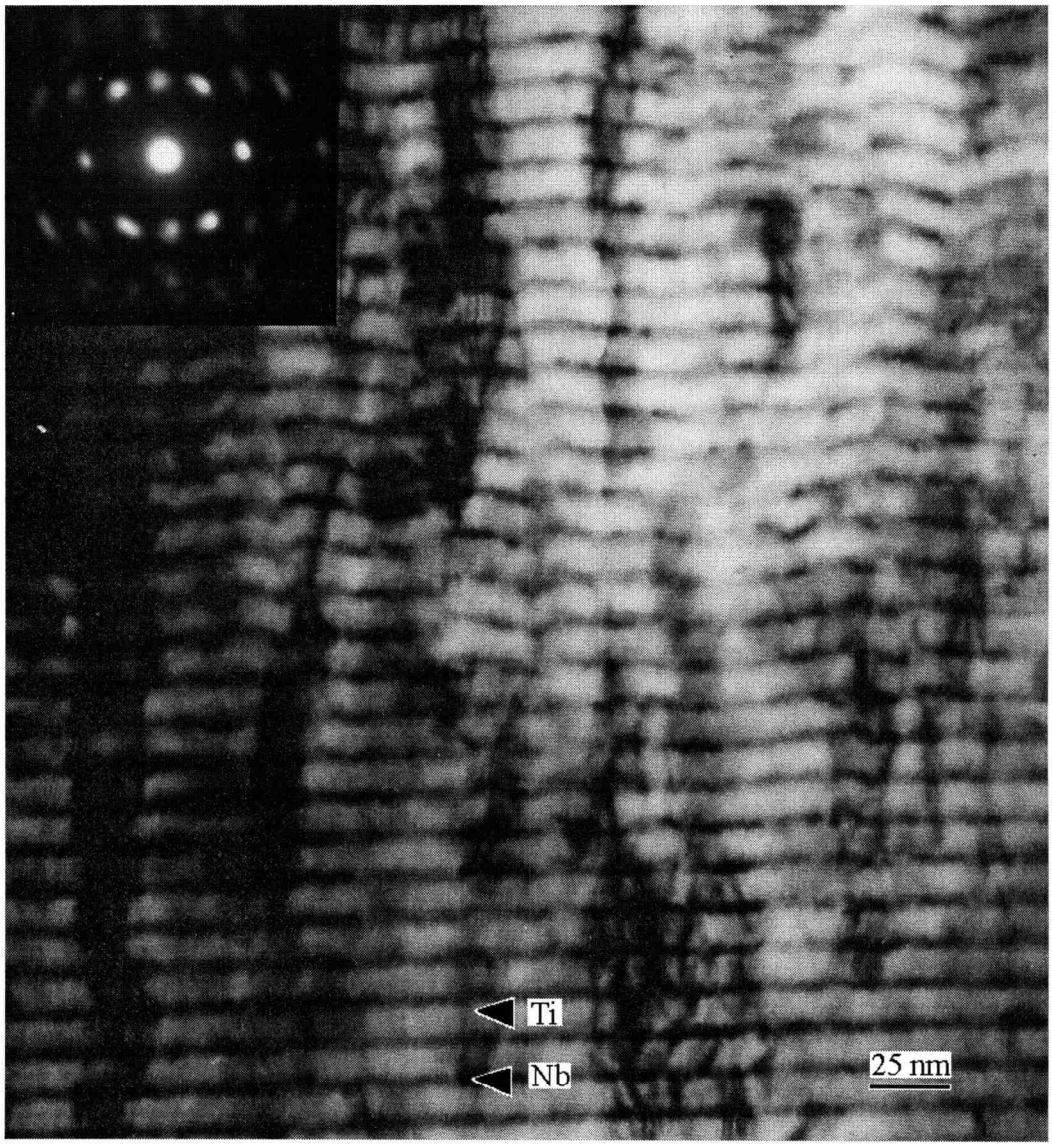

Figure 17. TEM Cross section and SAD of NbTi multilayer after 10 hours at 300°C.

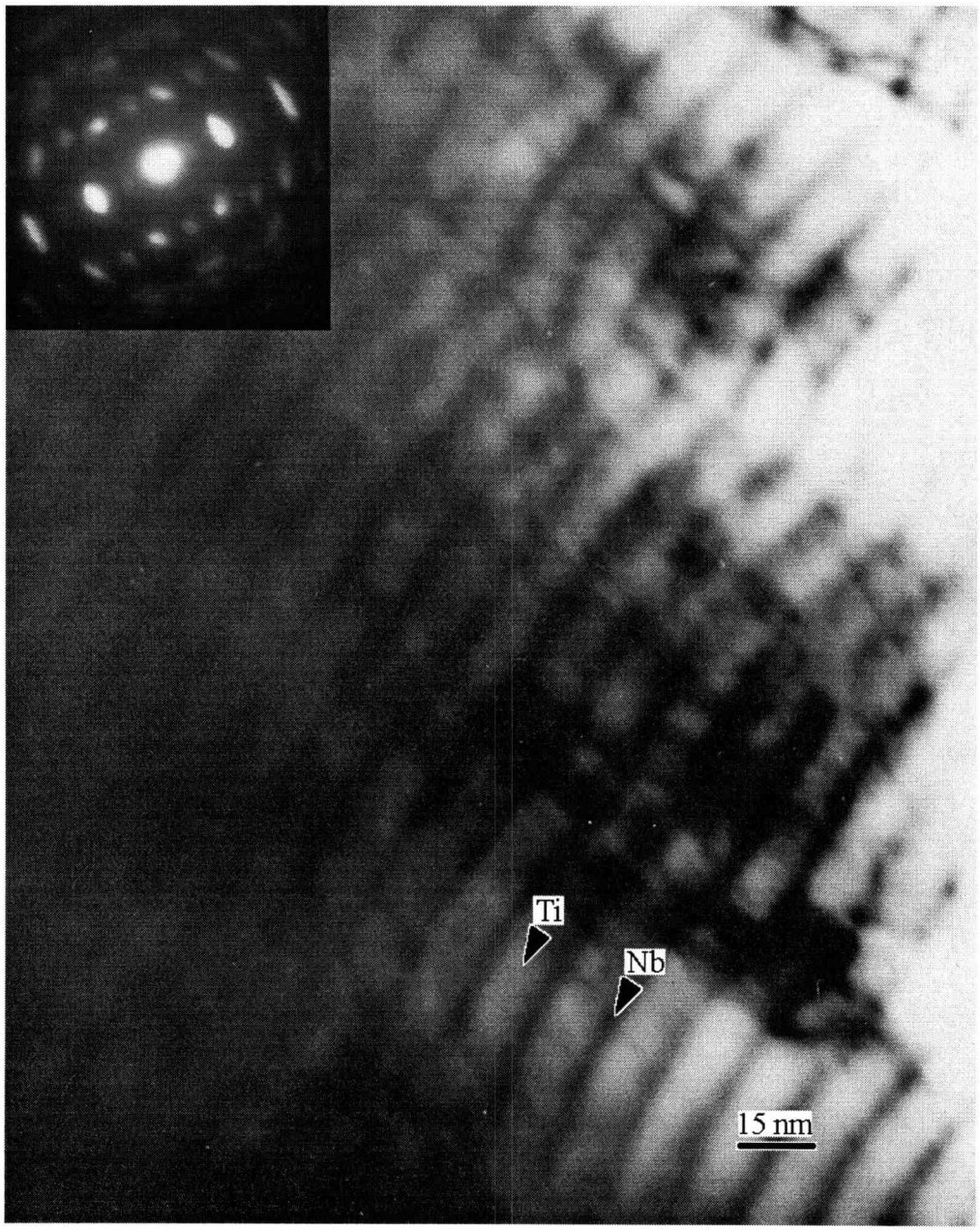

Figure 18. TEM Cross section and SAD of NbTi multilayer after 10 hours at 400°C.

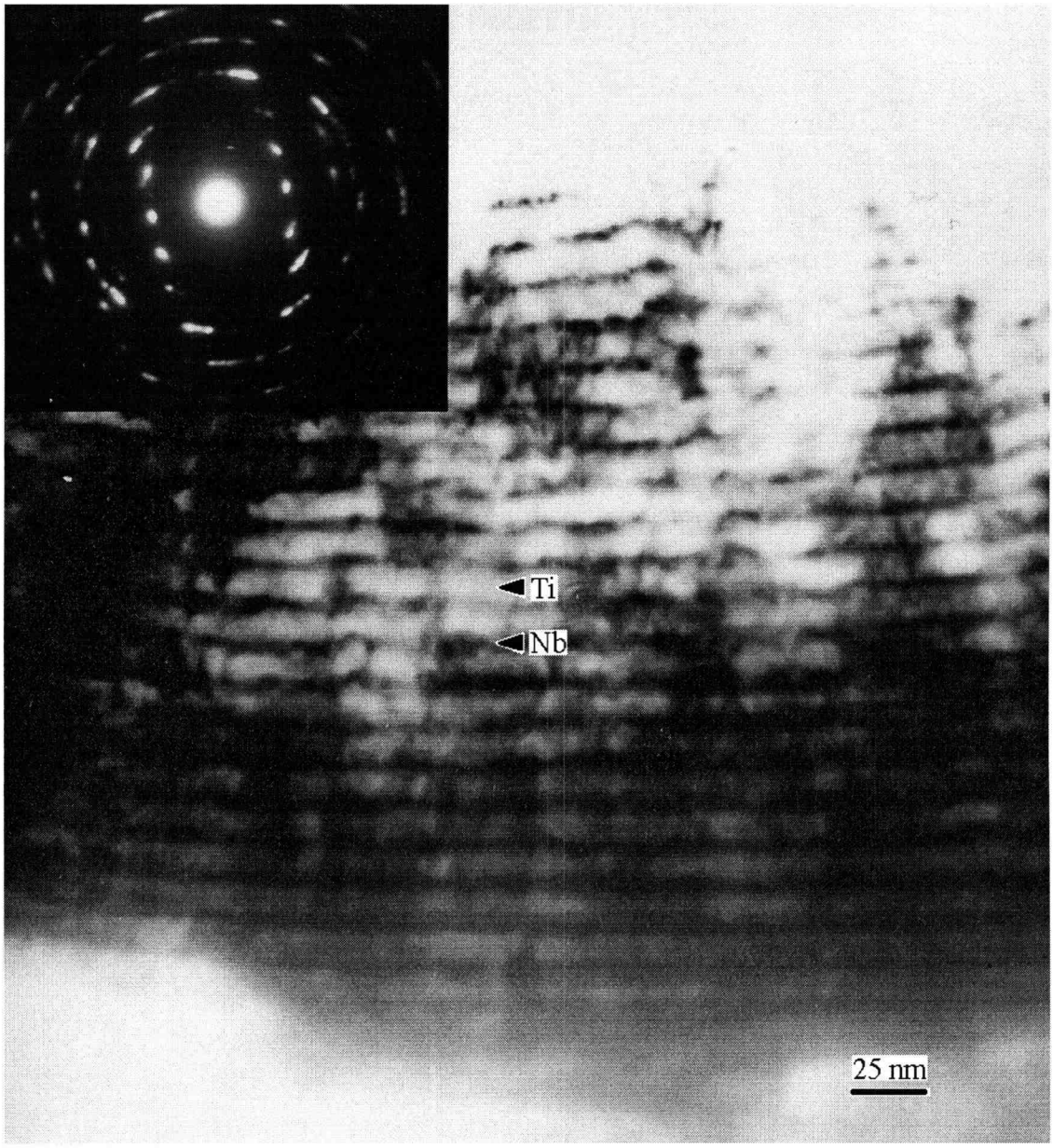

Figure 19. TEM Cross section and SAD of NbTi multilayer after 3 hours at 450°C.

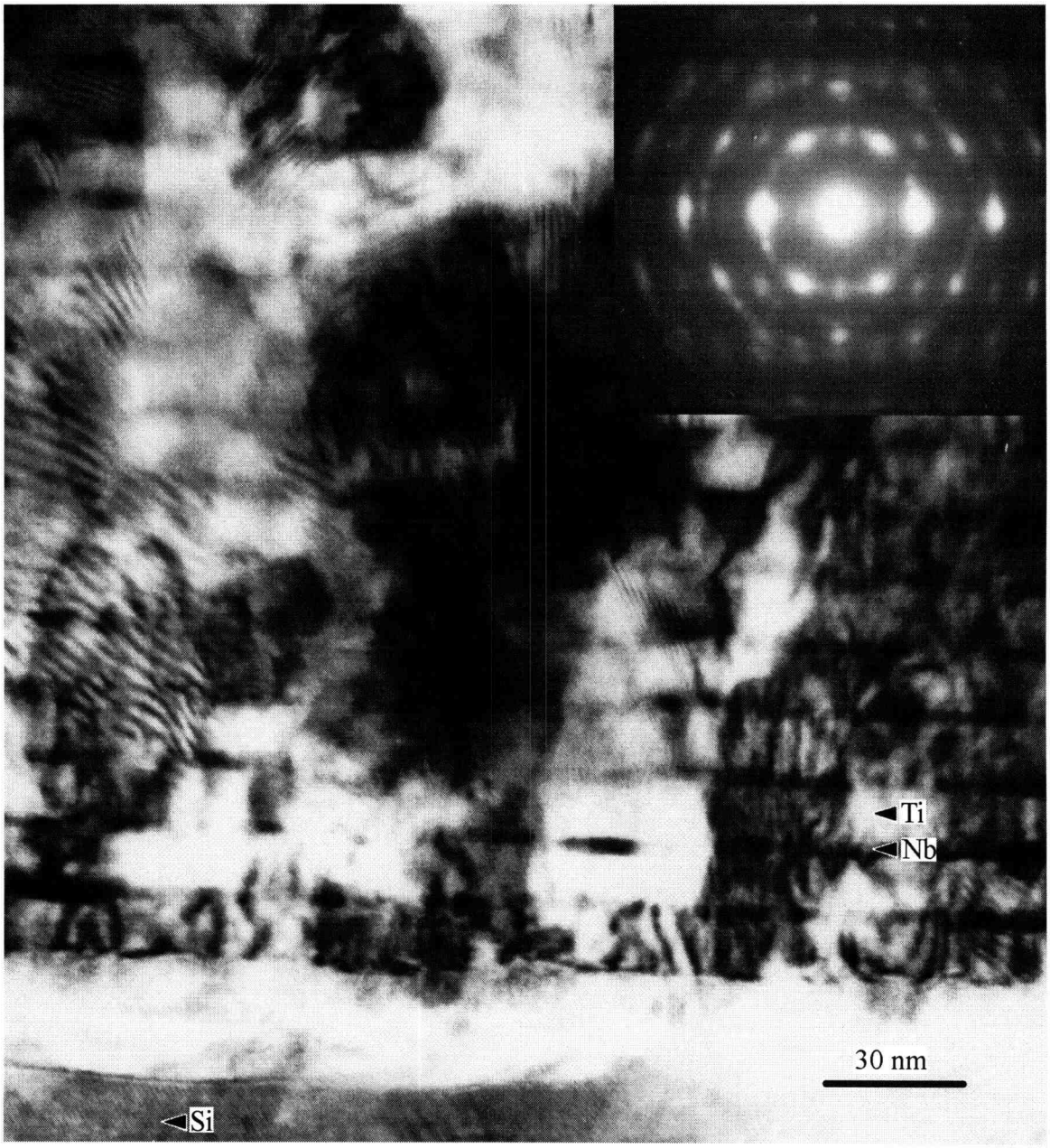

Figure 20. TEM Cross section and SAD of NbTi multilayer after 10 hours at 450°C.

4.1.4 Resistivity and RRR

Table 6 lists the resistivity and residual resistivity ratio of all NbTi samples. The resistivity of all NbTi samples was less than half the values reported by Zheng *et al* (1981). The change in resistivity, $\frac{\partial \rho}{\partial T}$, for all samples was negative between 298 and 77 K and positive between 77 and 4.2 K. Fisk and Lawson (1973) suggest that this behavior occurs when scattering is dominated by impurities or vacancies, and the phonon scattering effects are obscured.

Another explanation for the resistivity behavior is that one or both of the components of the multilayer exhibits semimetallic behavior. The original, as deposited multilayer does appear to be highly disordered, as evidenced in the SAD patterns obtained from TEM. However, following the heat treatments, recrystallization (reordering) has occurred. The resistivity behavior exists even on the fully interdiffused sample (1 hour 600°C).

Table 6. Resistivity and Residual Resistivity Ratio of Heat Treated NbTi Multilayers

Sample	ρ_{RT} (μΩ cm)	ρ_{LN2} (μΩ cm)	ρ_{LHe} (μΩ cm)	RRR
No Heat Treatment	39.7	-	46.3	0.86
1 hour 300°C	32.3	36.5	35.8	0.90
3 hours 300°C	31.1	34.1	30.2	1.03
10 hours 300°C	34.6	41.2	37.5	0.92
1 hour 400°C	33.6	40.8	36.1	0.93
3 hours 400°C	32.0	36.6	36.0	0.89
10 hours 400°C	30.7	32.2	29.8	1.03
1 hour 450°C	31.9	37.3	35.4	0.90
3 hours 450°C	34.2	40.3	39.8	0.86
10 hours 450°C	29.6	35.9	36.5	0.81
1 hour 600°C	37.0	43.1	39.4	0.94

4.1.5 Superconducting Properties

Table 7 lists the T_c predictions made for all heat treated samples for the interlayer thickness' predicted from the diffusion model. The T_c's were obtained using the Ledvij *et al* (1988) proximity effect model using a coherence length ξ of 15 Å.

Table 8 lists the measured superconducting properties of all samples. Samples heat treated at 400°C for 3 hours and above and all samples heat treated at 450°C and

600°C show superconducting properties at or above 4.2 K. Samples heat treated for 3 and 10 hours at 400°C and for 1 and 3 hours at 450°C show T_c's at or slightly above 4.2 K. The sample heat treated for 10 hours at 450°C shows a T_c at 5.48 K. The sample heat treated for 1 hour at 600°, which completely interdiffused the multilayer, had a T_c of 7.61 K. Although this alloy T_c is lower than expected for Nb47 % Ti, it was used in the prediction calculations using the Ledvij *et al* model. The T_c for Nb was assumed to be 9.2 K.

Table 7. Prediction of T_c's based on interlayer thickness' from diffusion model.

Sample	Interlayer Thickness	Predicted T_c (K)	Actual T_c (K)
1 hour 300°C	0.4 Å	2.66	<4.2
3 hours 300°C	0.6 Å	2.74	<4.2
10 hours 300°C	0.6 Å	2.74	<4.2
1 hour 400°C	1.8 Å	3.10	<4.2
3 hours 400°C	3.9 Å	3.66	4.3
10 hours 400°C	6.8 Å	4.32	4.4
1 hour 450°C	7.5 Å	4.44	4.3
3 hours 450°C	20 Å	7.64	4.2
10 hours 450°C	64 Å	7.76	5.5
1 hour 600°C	100%	7.61	7.6

Table 8. Superconducting Properties of Heat Treated NbTi Multilayers

Sample	H_{c2} (Tesla)	Transition Width (Tesla)	J_c at (Amps/mm^2)	Field (Tesla)	T_c (K)
No Heat Treatment	-	-	-	-	**<4.2 K**
1 hour at 300°C	-	-	-	-	**<4.2 K**
3 hours at 300°C	-	-	-	-	**<4.2 K**
10 hours at 300°C	-	-	-	-	**<4.2 K**
1 hour at 400°C	-	-	-	-	**<4.2 K**
3 hours at 400°C	0.4	± 0.2	-	-	**4.31 ± 0.16**
10 hours at 400°C	0.3	± 0.2	9	0.09	**4.42 ± 0.15**
1 hour at 450°C	1.1	± 0.6	10.6 4.4	0.4 0.5	**4.30 ± 0.20**
3 hours at 450°C	2.3	± 1.3	9.6 3.32 0.07	0.8 1.0 1.3	**4.19 ± 0.14**
10 hours at 450°C	5.7	± 0.9	5.72 4.04 2.44 1.81	4.00 4.25 4.50 4.75	**5.48 ± 0.22**
1 hour at 600°C	8.4	unknown	9.35 5.80 1.57	7.75 8.00 8.25	**7.61 ± 0.09**

The upper critical field increases with increasing heat treatment. The transitions of upper critical field are relatively wide. Figure 21 shows a normalized plot of upper critical field for all superconducting samples. Critical currents are listed for comparison.

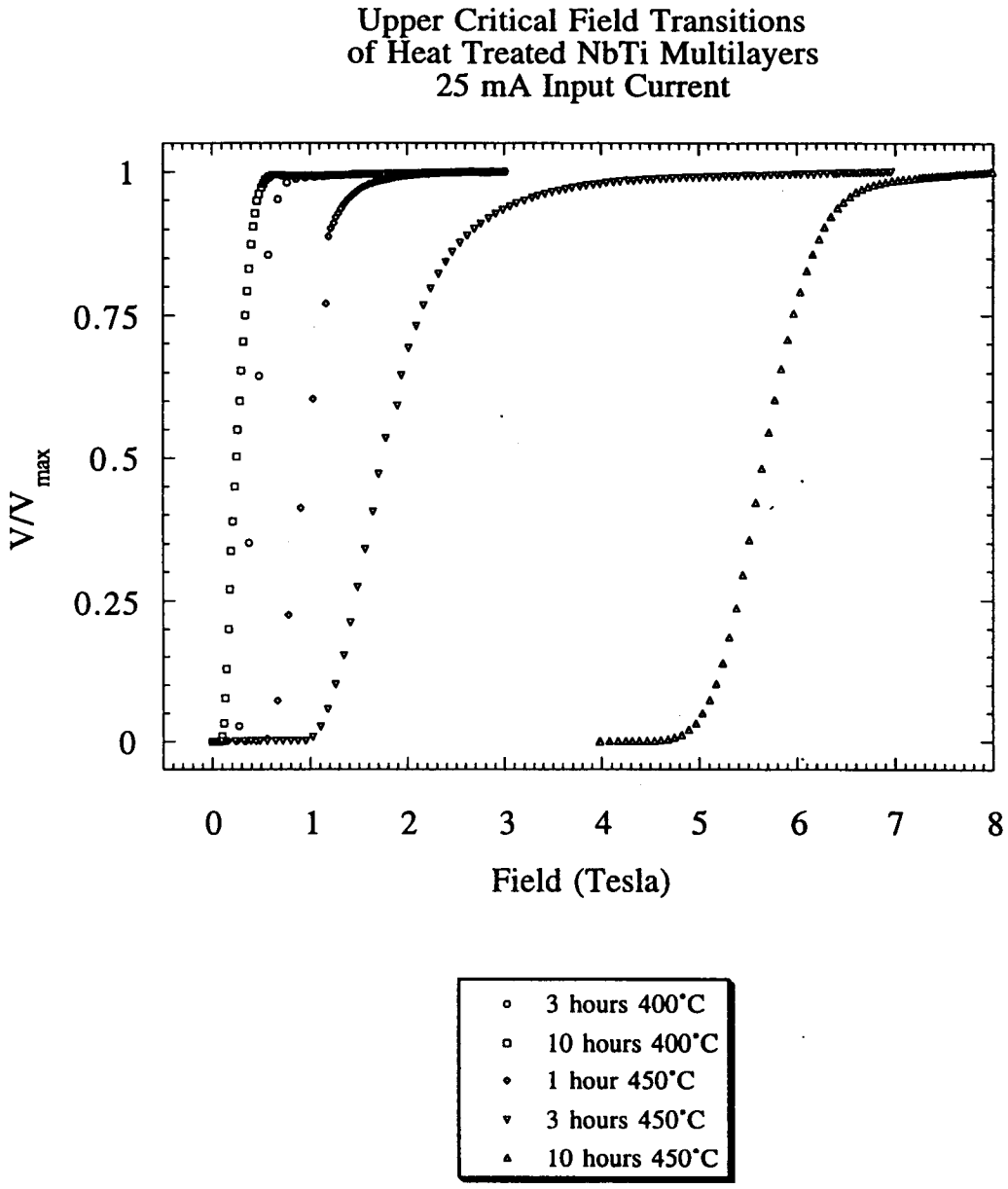

Figure 21. Upper critical field transitions of heat treated NbTi multilayer.

4.2 Conclusions

The diffusion model predicted a stable multilayer structure through all heat treatments between 1 hour at 300°C and 10 hours at 450°C. The model also predicted complete interdiffusion of the multilayer for the 1 hour at 600°C heat treatment. Adequate atomic mobility was predicted at the low temperature heat treatments. This atomic mobility was sufficient to increase the order within the multilayer as evidenced by the reduction in the width of the selected area diffraction ring and an increased spotting in the ring. The model also predicted a reduction in the concentration gradient at the niobium and titanium interface, effectively reducing the phase contrast. This resulted in the reduction of the intensities of the small angle superlattice peaks, though the compositional modulation remained intact. The predicted interlayer thicknesses were used to predict the general increasing T_c trend.

X-ray diffraction confirmed the existence of the multilayer structure as evidenced by the small angle superlattice peaks. High angle XRD and the Sherrer calculations shows a grain size or phase coherence of 5-20nm, on the order of the bilayer period. This is in rough agreement with the TEM results. X-ray diffraction confirms that there was still a strong modulated composition for all samples except the 1 hour 600°C sample. TEM also confirms the multilayer structure of the samples. There is evidence for non-uniform diffusion in select regions of the multilayer.

Transmission Electron microscopy also confirmed the multilayer structure and bilayer period which match the XRD results. The multilayer structure was stable over the range of diffusion up through 10 hours at 450°C. There is evidence, however, of a

silicide growth at the NbTi/Si interface and therefore potential contamination of Si into the NbTi by diffusion. From the TEM photos, the multilayer structure begins uniformly at the silicon interface, but increasingly roughens as more layers are deposited.

The resistivity behavior of the films can be explained by the dominate scattering from impurities or vacancies. However, if the vacancy concentration were higher than normal, increased amounts of interdiffusion would be expected. There is no evidence of faster than expected interdiffusion. The resistivity can also be due to scattering at the interfaces. Regardless of the cause, the electron transport problems with this multilayer may account for the low T_c's of all samples, including the sample heat treated for 1 hour at 600°C.

The T_c's measured for all samples were lower than expected for bulk Nb47$^{w}/_{o}$Ti, but increase with increasing heat treatment. This is probably due to a combination of the electron transport problems and possible contamination from either oxygen or silicon. The increasing T_c's predicted from the diffusion calculations are in direct agreement with the increasing interlayer of the Ledvij *et al* trilayer model. The H_{c2} of all superconducting samples were affected by the low T_c's. The J_c's were very low for the all superconducting samples.

5. FUTURE WORK

The future work ahead of this project is extensive, and unfortunately, my work with the experimentation has come to an end. It is appropriate to restate here that the whole reason for creating these multilayers was to study an engineered microstructure and its effect on flux pinning. The poor T_c's of this first set of multilayers only created a temporary setback. Ultimately, I am convinced that the priority of future work should be toward alloy target deposition of NbTi/Ti multilayers. Deposition can be conducted at temperatures as high as 300°C without significant interdiffusion. This would allow increased atomic mobility for surface reordering during deposition not obtained with this set of multilayers. Ideally, this would maximize the T_c of the multilayer at or near 9.3 K. Higher J_c's and H_{c2}'s would theoretically follow suit.

In order to acquire an acceptable flux pinning set of multilayers, the deposition process must be further characterized. Since this thesis was written, multilayers of Nb/Ti with bilayer periods of one-tenth and ten times the period of this sample set were prepared at Lawrance Livermore National Laboratories. These multilayer films will provide insight into proximity effect coupling theory, as well as furthur verification of the diffusion model.

The diffusion model itself needs to be refined to incorporate the non-linear regions of the prefactor and activation energies from the empirical data. As it stands now, the model should be presented to the scientific literature as a means of predicting

binary diffusion. The model is calculation intensive, but with the advances in computer technology, this is hardly a deterrent any more.

To enhance the characterization of these and future multilayers, several, more thorough measurements need to be done. T_c measurements below 4.2 K need to be conducted. This would give substantial information with regard to proximity effect depression of T_c. Resistivity measurements should also be conducted through the full range of temperatures down to T_c. High resolution electron microscopy should also be done to examine the lattice strain and interlayer spacing of as deposited and heat treated multilayers.

BIBLIOGRAPHY

Abrikosov, A.A., 1957, Sov. Phys. JETP, v5, p1174.

An, H., Yuan-Hang, W., Xiang-Jin, L., Zheng, Y., and Duan, F., 1986. Phys. Stat. Sol., v98, p215.

Broussard, P.R., 1986. Ph.D. Thesis. Stanford University.

Campbell, A.M., and Evetts, J.E., 1972. Adv. Phys., v21, p199.

Carcia, P.F., and Suna, A., 1983. J. Appl. Phys. v54, p2000.

Carter, G.F., 1979. Principles of Physical and Chemical Metallurgy, American Society for Metals

Cook, H.E., and Hilliard, J.E., 1969. J. Appl. Phys., v40, p2191.

Cooper, L., 1961. Phys. Rev. Let., v6, p698.

Crank, J., 1975. The Mathematics of Diffusion, 2nd Ed., Oxford.

de Gennes, P.G., 1964. Rev. Mod. Phys., v123, p225.

Dew-Hughes, D., 1974. Philos. Mag., p293.

Essman, U., and Trauble, H., 1967. Phys. Lett., v24A, p526.

Fisk, Z., and Lawson, A.C., 1973. Sol. St. Comm. v13, p277.

Gibbs, G.B., Graham, D., and Tomlin, D.H., 1963. Philos. Mag., v8, p1269.

Gurvitch, M., 1986. Phys. Rev. B., v34, p540.

Koch, C.C., Scarbrough, J.O., and Kroeger, D.M., 1974. Phys. Rev. B, v9, p888.

Larbalestier, D.C., 1981. Superconductor Materials Science, Plenum.

Ledvij, M., Dobrosavljevic-Grujic, L., and Clem, J.R., 1988. Phys. Rev. B, v38, p129.

Matsumoto, K., Tanaka, Y., Yamafuji, K., Funaki, K., Iwakuma, M., and Matsushita, T., 1993. IEEE Trans. Appl. Superconductivity, MJ-6.

Meingast, C., Lee, P.J., and Larbalestier, D.C., 1989. J. Appl. Phys., v66, p5962.

Moffat, D.L., Ph.D. Thesis, University of Wisconsin-Madison, unpublished, 1985.

Pontau, A.E., and Lazarus, D., 1979. Phys. Rev. B, v19(8), p4027.

Qian, Y.J., Zheng, Q., Sarma, B.K., Yang, H.Q., Ketterson, J.B., and Hilliard, J.E., 1982. J. Low Temp. Phys., v49, p279.

Radovic′, Z., Ledvij, M., and Dobrosavljevic′-Grujic′, L., 1991. Phys. Rev. B, v43, p8613.

Sato, N., 1990. J. Appl. Phys., v67, p7493.

Silvert, W., 1975. J. Low Temp. Phys., v20, p439.

Slaughter, J.M., Schulze, D.W., Hills, C.R., Mirone, A., Stalio, R., Watts, R.N., Tarrio, C., Lucatorto, T.B., Krumrey, M., Mueller, P., and Falco, C.M., 1994. J. Appl. Phys., v76, p2144.

Ullmaier, H., 1975. Irreversible Properties of Type II Superconductors, Springer -Verlag, NY.

Werner, T.R., Banerjee, I., Yang, Q.S., Falco, C.M., Schuller, I.K., 1982. Phys. Rev. B. v26, p2224.

Werthamer, N.R., 1963. Phys. Rev., v132, p2440.

Zerweck, G., 1981. J. Low Temp. Phys., v42, p1.

Zheng, J.Q., Ketterson, J.B., Falco, C.M., and Schuller, I.K., 1981. Physica B, v108, p945.

Zhou, R., Hong, S., and Marancik, W., 1993, IEEE Trans. Appl. Superconductivity, MCA-2.

APPENDIX

Binary Diffusion Code

The following C code was written by the author to model the time dependent diffusion of the two metals of the multilayer during heat treatments.

```
#include <stdio.h>
#include <math.h>
                                /*Diffusion Program*/
                                /*Calculates the composition of a Multilayer*/
                                /*Thin Film (NbTi) as a function of temperature*/
                                /*and time*/
double T;                       /*GLOBAL  Temperature variable*/
double Delx = 5E-10;            /*GLOBAL Delta x spacing*/
double Time;                    /*GLOBAL Anneal Time */
int aneal_T;                    /*GLOBAL Temper. for save file name */
double Delt;                    /*GLOBAL Delta t spacing*/
int nodes=18;
double TiD_calc(double);        /* GLOBAL     Ti Diffusivity Function */
double NbD_calc(double);        /* GLOBAL     Nb Diffusivity Function */

main()
{
        int i,j,s;
        double max_t;
        double S_time;          /*How often (in time) to save data*/
        double Sav_Times;       /*number of Nbc files generated */
        double *pNbc;           /*pointer to Nbc array*/
        double *pNewNbc;
        double *pTic;           /*pointer to Tic array*/
        double *pNewTic;
        double *pNbf;           /*pointer to Nbf array*/
        double Nbc[nodes];      /*Nb composition array*/
        double NewNbc[nodes];
        double Tic[nodes];      /*Ti composition array*/
        double NewTic[nodes];
        double Nbf[nodes];      /*Nb atomic fraction array*/
        char Nbfile[20];
        char Tifile[20];
        FILE *Nbp,*Tip;

        double inTemp(void);    /*      Anneal Temperature    */
        double inTime(void);    /*Inputs:  Duration of Anneal    */
        double indelt(void);                    /*      increment in time (dt)*/
```

```
    double often_save(void);                    /*      How often to save    */
    double square_gen(double*,double*);         /*Generates a square wave   */
                                                /*for initial concentrations*/
    double afrac_calc(double,double);           /*Calculator of Nb atom fract'n*/
    double Nbc_calc(double*,double*,double*);
    double Tic_calc(double*,double*,double*);
    double Nb_Savefunct(double,double*);
    double Ti_Savefunct(double,double*);

    T = inTemp();
    aneal_T = T - 273;
    Time = inTime();                            /*Total anneal time MINUTES*/
    Delt = indelt();                                /*time step SECONDS*/
    S_time = often_save();                      /*Save every (S_time) minutes*/
    max_t=(S_time*60/Delt);
    Sav_Times = Time/S_time;
    pNbc = Nbc;                                 /*pNbc points to Nbc[0]*/
    pNewNbc = NewNbc;
    pTic = Tic;                                 /*pTic points to Tic[0]*/
    pNewTic = NewTic;
    pNbf = Nbf;                                 /*pNbf points to Nbf[0]*/
    square_gen(pNbc,pTic);                      /*Generates initial compositions*/
    Nb_Savefunct(0,pNbc);
    Ti_Savefunct(0,pTic);

                                        /*####START CALCULATION#####*/
for(s=1;s<Sav_Times+1;s++){

    for(j=0;j<max_t;j++){

        Nbc[0]=Nbc[2];                          /*    Ghost Nodes     */
        Nbc[nodes-1]=Nbc[nodes-3];              /*   for symmetric    */
        Tic[0]=Tic[2];                          /*  boundary conditions */
        Tic[nodes-1]=Tic[nodes-3];              /*                      */

            for(i=0;i<nodes;i++){               /*Calculates Nb atom.frac*/
                Nbf[i] = afrac_calc(Nbc[i],Tic[i]);
            }
        Nbc_calc(pNbc,pNewNbc,pNbf);
        Tic_calc(pTic,pNewTic,pNbf);
        for(i=1;i<nodes-1;i++){
            Nbc[i] = NewNbc[i];
            Tic[i] = NewTic[i];
        }
    }
```

```
        Nb_Savefunct(s*j*Delt/60,pNbc);
        Ti_Savefunct(s*j*Delt/60,pTic);
        printf("Timenow = %lf\n",s*j*Delt/60);
    }


        printf("Number of supposed saves = %lf\n",Sav_Times);
}

double Nb_Savefunct(double time, double *Nb_c)
{
        int i;
        int timenow;
        char filename[20];
        FILE *ofp;
        timenow = time;
        sprintf(filename,"%dNb%d.cnc%c",aneal_T,timenow,0);
        ofp = fopen(filename,"w");
        for(i=1;i<nodes-1;i++){
                fprintf(ofp,"%lf\n",*(Nb_c+i));
        }
        for(i=2;i<nodes-2;i++){
                fprintf(ofp,"%lf\n",*(Nb_c+nodes-1-i));
        }
        fclose(ofp);
}

double Ti_Savefunct(double time, double *Ti_c)
{
        int i;
        int timenow;
        char filename[20];
        FILE *ofp;
        timenow = time;
        sprintf(filename,"%dTi%d.cnc%c",aneal_T,timenow,0);
        ofp = fopen(filename,"w");
        for(i=1;i<nodes-1;i++){
                fprintf(ofp,"%lf\n",*(Ti_c+i));
        }
        for(i=2;i<nodes-2;i++){
                fprintf(ofp,"%lf\n",*(Ti_c+nodes-1-i));
        }
        fclose(ofp);
}
```

```
double Nbc_calc(double *Nb_c, double *NewNb_c, double *Nb_a)
{
        int k;
        double Nbterm1,Nbterm2,Nbterm3,crit1;
        crit1 = Delt/(2*pow(Delx,2));
  for(k=1;k<nodes-1;k++){
  Nbterm1 = NbD_calc(*(Nb_a+k-1)) + NbD_calc(*(Nb_a+k));
  Nbterm1 *=crit1;
  Nbterm2 = NbD_calc(*(Nb_a+k-1)) + 2*NbD_calc(*(Nb_a+k)) +
NbD_calc(*(Nb_a+k+1));
  Nbterm2 *=crit1 * (-1);
  Nbterm2 += 1;
  Nbterm3 = NbD_calc(*(Nb_a+k)) + NbD_calc(*(Nb_a+k+1));
  Nbterm3 *=crit1;
  *(NewNb_c+k) = *(Nb_c+k-1) * Nbterm1;
  *(NewNb_c+k)+= *(Nb_c+k) * Nbterm2;
  *(NewNb_c+k)+= *(Nb_c+k+1) * Nbterm3;
  }
}

double Tic_calc(double *Ti_c, double *NewTi_c, double *Nb_a)
{
        int k;
        double Titerm1,Titerm2,Titerm3,crit1;
        crit1 = Delt/(4*pow(Delx,2));
  for(k=1;k<nodes-1;k++){
  Titerm1 = TiD_calc(*(Nb_a+k-1)) + TiD_calc(*(Nb_a+k));
  Titerm1 *=crit1;
  Titerm2 = TiD_calc(*(Nb_a+k-1)) + 2*TiD_calc(*(Nb_a+k)) +
TiD_calc(*(Nb_a+k+1));
  Titerm2 *=crit1 * (-1);
  Titerm2 += 1;
  Titerm3 = TiD_calc(*(Nb_a+k)) + TiD_calc(*(Nb_a+k+1));
  Titerm3 *=crit1;
  *(NewTi_c+k) = *(Ti_c+k-1) * Titerm1;
  *(NewTi_c+k)+= *(Ti_c+k) * Titerm2;
  *(NewTi_c+k)+= *(Ti_c+k+1) * Titerm3;
  }
}
```

```
double afrac_calc(double Nb_conc,double Ti_conc)
        {
        int i;
        double Nb_atomfrac;
        Nb_atomfrac = Nb_conc/(Nb_conc+Ti_conc);

        return Nb_atomfrac;
        }

/*Generates initial Composition (determined to be a square wave)*/
double square_gen(double *Nb_conc,double *Ti_conc)
        {
        int i,j;
        for(i=0;i<12;i++){              /* Titanium rich region (start)*/
                *(Nb_conc+i) = 0;       /*sets Nb conc. to        */
                                        /*zero in Ti region       */
                *(Ti_conc+i) = 5.6607;          /*sets Ti conc. to        */
                                        /* 5.6607x10^28 atoms/m^3  */
                }
        for(i=12;i<nodes;i++){          /* Niobium  rich region (start)*/
                *(Nb_conc+i) = 5.5409;          /*sets Nb conc. to        */
                                        /*5.5409x10^28 atoms/m^3   */
                *(Ti_conc+i) = 0;       /*sets Ti conc. to        */
                                        /*zero in Nb region       */
                }

        }
```

```
/*INPUTS SECTION (START) ##############################################*/
double inTemp(void)
        {
        double Temp;

        printf("Input the Anneal Temperature in Kelvin:\n");
        printf("Temp = ");
        scanf("%lf",&Temp);
        return Temp;
        }

double inTime(void)
        {
        double Time;

        printf("Input the Anneal Time in MINUTES:\n");
        printf("Time = ");
        scanf("%lf",&Time);
        return Time;
        }

double often_save(void)
        {
        double save_increment;

        printf("Input how often files will be saved in MINUTES:\n");
        printf("Time Increment = ");
        scanf("%lf",&save_increment);
        return save_increment;
        }

double indelt(void)
        {


        double delta_t;
        double maxdelta_t;
        double D;
        double Q;
        double NbD;
        double atomfrac;

        atomfrac = 0;                   /*Nb diffuses fastest into an alloy*/
                                        /*containing no Nb              */
        NbD = NbD_calc(atomfrac);
```

```
        maxdelta_t = (pow(Delx,2))/(2*NbD);
        printf("The maximum time step allowable is Delt = ");
        printf("%lf seconds",maxdelta_t);
        printf("\nWhat Delt SECONDS do you want to use?   Delt = ");
        scanf("%lf",&delta_t);

        return delta_t;
        }
/*INPUTS SECTION (END)  ##############################################*/

/*Diffusivity of Titanium into NbTi as a function of */
/*the atomic fraction of Nb present */

double TiD_calc(double atomfrac)
{
        double D;
        double Q;
        double TiD;

        D = 0.001663*exp(2.299*atomfrac);
        Q = 33991 + (54400 * atomfrac);
        TiD = (D * exp(-Q/(1.987*T)))*(1E-4);       /* units in */
                                                    /* m^2/s */
        return TiD;

}


/*Diffusivity of Niobium into NbTi as a function of */
/*the atomic fraction of Nb present */

double NbD_calc(double atomfrac)
{
        double D;
        double Q;
        double NbD;

        D = 5.5783E-4*exp(8.209*atomfrac);
        Q = 31463 + (65740 * atomfrac);
        NbD = (D * exp(-Q/(1.987*T)))*(1E-4);       /* units in */
                                                    /* m^2/s */
        return NbD;
}
```